Energy & Environmental Science

Cite this: *Energy Environ. Sci.*, 2011, **4**, 818

www.rsc.org/ees

REVIEW

Solution-derived ZnO nanostructures for photoanodes of dye-sensitized solar cells

Feng Xu and Litao Sun*

Received 17th September 2010, Accepted 9th November 2010
DOI: 10.1039/c0ee00448k

Solution-phase derived ZnO nanostructures have triggered considerable interest and become the mainstream route to obtain low-cost and large-scale electrode materials for dye-sensitized solar cells (DSSCs). The article reviews recent progress in liquid-phase synthesis methods for preparing ZnO nanostructures as the photoanodes of the DSSCs. A few classic paradigms and new advancements in the ZnO nanostructures made by our group are demonstrated. The effects of ZnO nanostructured films with different morphologies, prepared by solution-phase approaches, on the performance of DSSCs are discussed. Finally, various liquid-phase methods of ZnO nanostructure synthesis are summarized and compared to allow further exploration of the ways to improve the photoelectric conversion efficiency of DSSCs.

1. Introduction

Increasing world demand for energy is expected to double within the next 50 years, and triple by the end of this century.[1] However, the supply of fossil fuels will not be able to keep up with the growing demand in a sustainable way. In order to maintain social and economic development, people must intensify efforts on finding highly effective and renewable energy sources. To date, various renewable energy sources from the nature such as wind power, water power, biofuel, tide, terrestrial heat, and sunshine flux,[2–9] have been used to make our world continuously work. In total, these renewable sources take up nearly one eighth of all energy production,[10] and the percentage is expected to keep an impressive annual growth in the next decades. But, due to regional limitations, the energy derived from wind power, water power, biofuel, tide and terrestrial heat cannot be available to all people throughout the world. In this regard, light flux from the sun is the most ideal energy source. Sunlight provides the largest of all carbon-neutral energy sources, and one hour of sunshine yields an energy that almost amounts to a whole year of global consumption.[11] Therefore, solar energy is commonly considered to be the ultimate solution to our need for clean, abundant, and renewable energy resources in the future.

Solar power can be converted directly into electrical power by photovoltaic (PV) solar cells. The first modern PV solar cells based on single-crystalline silicon (Si) were developed by Chapin *et al.* at the Bell Laboratory in 1954.[12] Single-crystalline Si solar cells follow the principle of p–n junctions, formed by joining

SEU-FEI Nano-Pico Center, Key Laboratory of MEMS of Ministry of Education, Southeast University, Nanjing, 210096, China. E-mail: slt@seu.edu.cn; Fax: +86-25-83792939; Tel: +86-25-83792632 ext. 8813

Broader context

The dye-sensitized solar cell (DSSC) is a wonderfully successful paradigm that mimics natural photosynthesis where chlorophyll absorbs photons but does not participate in charge transfer. This is different from traditional photovoltaic cells where semiconductors assume both the functions. In DSSCs, the dye-sensitized nanocrystalline semiconductor films act as photoanodes and play a significant role in converting photons into electrical energy. Light harvesting, electron injection and collection, and unwanted electron recombination are all correlated with the photoanode. TiO_2 nanoparticles have been widely used as photoanode materials in DSSCs, but suffer from high recombination losses and low electron transport properties. Therefore, new materials and architectures are sought to further improve the performance of DSSCs. In this regard, ZnO, with its wide variety of nano-forms synthesized through facile and scalable techniques, is a fascinating alternative to TiO_2 due to having a similar lowest conduction band edge and higher electronic mobility. This review mainly focuses on recent progress in solution synthesis methods for preparing ZnO nanostructures as the photoanodes of the DSSCs. The advantages and disadvantages of various solution synthesis methods are analyzed in order to further develop ways to optimize the performance of photoanodes, and thus improve the photoelectric conversion efficiency of DSSCs.

p-type and n-type semiconductors. The electrons and holes are generated by photo-excitation at the interface of a p–n junction, separated by the electrical field across the junction, and collected through external circuits. Later on, poly-crystalline Si was also developed and used to prepare PV solar cells. However, the purification of crystalline Si from quartz and sand in nature is a rather energy-demanding process, which greatly increases the production cost of PV solar cells based on single/poly-crystalline Si. Considering the extremely high material cost, thin-film solar cells have been developed with the aim of reducing production costs.[13–15] The first amorphous Si thin-film solar cell was born in 1976.[16] Due to its higher light-absorption efficiency compared to crystalline Si, an amorphous Si thin-film does not need an Si layer as thick as crystalline Si, thus cutting down the amount of Si used. Unfortunately, the amorphous Si-based solar cells have encountered a development bottleneck due to the Staebler–Wronski light induced degradation effect.[17] This photoelectronic effect may result in a loss of cell efficiency of up to 50% or more.

Besides amorphous Si thin-film materials, other PV thin-film semiconductor materials such as CdTe,[18–22] $CuInSe_2$ (CIS),[23] and $CuInGaSe_2$ (CIGS),[24] have also been used in solar cells, and have obtained single-junction conversion efficiencies of 16–32%.[25] To attain higher conversion efficiency, GaAs and InGaP III–V semiconductor multijunction solar cells[26] have been devised to take full advantage of the whole solar spectrum. Especially in space applications, where cost is not major problem, multi-junction cells have replaced Si ones. Currently, CIGS solar cells, along with amorphous Si and CdTe ones, are the leading thin-film technology. These PV devices have the same working principle as crystalline Si-based ones and make use of one or more p–n junctions to absorb photons. Although the above-mentioned PV solar cells based on Si or compound semiconductors have achieved relatively high efficiencies for practical use, they still require major breakthroughs to meet the long-term goal of low production and operating cost. In this respect, dye-sensitized solar cells (DSSCs), as a third-generation photoelectrochemical (PEC) cell with an entirely different working principle from crystalline Si-based ones, have emerged as a promising alternative for low-cost energy production.

The DSSC is a wonderfully successful paradigm that mimics natural photosynthesis, where chlorophyll absorbs photons but does not participate in charge transfer.[11,27] This situation is different from the traditional PV cells where semiconductors assume both the functions. A typical DSSC is composed of two sheets of glass coated with a transparent conductive oxide (TCO) layer. One of the glass sheets is covered with a film of porously structured semiconductor particles with adsorbed dye molecules as the sensitized photoanode (the working electrode). The other glass sheet is coated with a catalyst (commonly metal platinum or carbon) which acts as the counter electrode (*i.e.* the cathode). The electrodes are then sandwiched together and the electrolyte, commonly a redox couple (I^-/I_3^-) in organic solvents, fills the interspace between them to serve as a conductor to electrically connect the two electrodes. An outline of the operation principle of the DSSC is illustrated in Fig. 1(a). First, photons from sunlight are captured by dye molecules (**S**), causing the dye photoexcitation (**S***), and excitons are rapidly split at the surface of semiconductor film. Then, electrons are injected into semiconductor film and reach the collector (TCO) by a series of interparticle hop steps through the semiconductor particle film. Afterwards, the electrons go through an outer circuit to reach the counter electrode, fulfilling the electrical mission on the way. Electrons are then transferred to the electrolyte where they reduce the oxidant species (**Ox**) with the aid of a catalyst. Subsequently, the formed reducing agent (**Red**) reduces the excited dye molecules (**S***) to the ground state (**S**), completing the whole cycle. Certainly, there are also inevitable processes which breach the expected operation of a DSSC: the excited dye can decay (either radiatively or nonradiatively) before it injects the electrons, the injected electrons within the photoanode can recombine with the oxidized dye before the dye is regenerated, or the redox couple can intercept an electron from the photoanode before electrons are collected. The desirable processes (electron injection, electron collection, and dye regeneration) and the

Feng Xu

Feng Xu received his BS and MS in Electrochemistry, and PhD in Materials Science and Engineering, from Nanjing University of Technology. In 2009 he joined the group of Prof. Litao Sun as a postdoctoral researcher at Southeast University (SEU). His research interests and expertise center on synthesis, TEM characterization and functionalization of nanomaterials, including semiconducting oxide and carbon materials and their application to photoelectrochemical and field emission devices.

Litao Sun

Prof. Dr Litao Sun received his PhD from the Shanghai Institute of Applied Physics, Chinese Academy of Sciences in 2005. From 2005 to 2008 he was a research fellow with Prof. Florian Banhart at the Institute of Physical Chemistry, University of Mainz. He returned to China in 2008, and became Distinguished Professor and vice dean of School of Electronic Science and Engineering at SEU. His research focuses on preparation, in situ TEM characterization, and device applications of nanomaterials. He is the author of around 100 papers and review articles in international journals including Science, Nat. Nanotech., PRL, Adv. Mater., Chem. Commun., and Small.

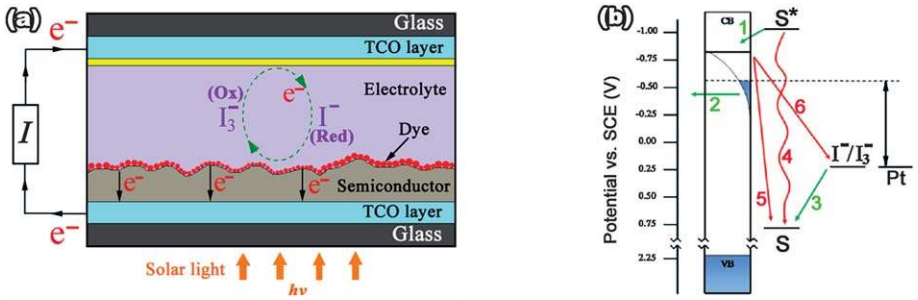

Fig. 1 (a) Principle of operation and energy level scheme of the dye-sensitized solar cell (DSSC); (b) approximate energy diagram of a typical DSSC based on TiO_2. Desirable processes (1. electron injection, 2. electron collection, 3. dye regeneration) are marked with green arrows and deleterious processes (4. luminescence or nonradiative decay, 5. recombination, 6. interception) are marked with red arrows.[28]

deleterious processes (luminescence or nonradiative decay, recombination, and interception) are marked with green and red arrows in Fig. 1(b),[28] respectively. In fact, the generation of electricity is the result of dynamic competition between the desirable and deleterious processes. An efficient cell module should facilitate the desirable processes and hinder the deleterious processes.

In DSSCs, the dye-sensitized nanocrystalline semiconductor film as a photoanode plays a significant role in converting photons into electrical energy. Light harvesting, electron injection and collection, and unwanted electron recombination are all correlated with the photoanode. So far, the most impressive DSSCs are the ones based on TiO_2 nanoscopic crystalline particle films loaded with a ruthenium–polypyridine complex dye (such as N3 and N719 dyes).[29] The work was first initiated by M. Grätzel and his coworkers who worked in Swiss Federal Institute of Technology in 1991, and a remarkable breakthrough in conversion efficiency (7.1–7.9%) was obtained.[30] Henceforth, the conversion efficiency was continually advanced, and a highest overall conversion efficiency of 11.18% has been achieved using the purified N719 photosensitizer adsorbed on TiO_2 films in its monoprotonated state.[31] Unfortunately, the record high conversion efficiency of DSSCs (11.18%) plateaued in an unchanged level over the following 15 years. Further increase in conversion efficiency is difficult due to large energy loss from serious recombination between electrons and either oxidized dye molecules or electron-accepting species in the electrolyte during the charge-transport process.[32–34] Such a recombination is related to the lack of a depletion layer on TiO_2 nanocrystallite surfaces,[35] and becomes comparatively serious as the thickness of TiO_2 photoanode film increases. Thus, more basic research is needed to alter the structure and/or nature of the components in the DSSCs, particularly in the semiconductor photoanode materials that bridge the dyes and the electron collecting anode, in order to optimize the electron-transfer energetics and kinetics. In this regard, the wide-band-gap semiconductor zinc oxide (ZnO) has attracted much attention as a fascinating alternative to TiO_2 photoanode in DSSCs. This is because ZnO and TiO_2 exhibit similar lowest conduction band edges and electron injection process from the excited dyes. Additionally, the lifetime of carriers in ZnO is significantly longer than that in TiO_2. More importantly, in comparison to TiO_2, ZnO has a higher electronic mobility which is favorable for electron transport. Therefore, it is expected that reduced recombination would be achieved when ZnO is used as photoanode in DSSC due to rapid electron transferring and collecting.

Currently, increasing interest has been focused on ZnO-based DSSCs, and many research groups all over the world have spent much effort on optimizing the components of ZnO-based DSSCs, such as the morphology of photoanode, the categories of dye and electrolyte, and the selection of the catalyst on counter electrode. Also, a large amount of studies on the performance parameters of DSSCs including open-circuit photovoltage (V_{oc}), short-circuit photocurrent (I_{sc}), and fill factor (FF) have been performed intensively. Based on these extensive investigations, at present, a highest conversion efficiency (η) of 6.58% has been triumphantly achieved.[36] Many researchers working on ZnO-based DSSCs expect that there is still huge potential to improve the cell conversion efficiency by further optimization in all aspects, especially the photoanode morphology of ZnO nanostructures. Due to the ease of crystallization and anisotropic growth of ZnO material, it embodies a wide variety of nanostructures, such as ZnO nanoparticles, one-dimensional (1D) nanowires/rods/tubes/fibers, 2D nanosheets/belts/plates, and 3D hierarchical structures. All these nanostructures have been successfully applied in ZnO-based DSSCs. These ZnO nanostructures can be fabricated by various techniques, including thermal evaporation,[37–39] dc plasma reaction,[40] chemical vapor deposition (CVD),[41] molecular beam epitaxy (MBE),[42] sputtering,[43] and solution-derived synthesis methods,[44] and so forth. Considering that DSSCs will hold the balance in the future energy production and take up a considerable market quotient in energy supply, ZnO nanostructured photoanodes should be constructed by some facile, low-cost and scale-up methods. Recently, many researchers have presented reviews on TiO_2-based or ZnO-based DSSCs.[45–63] According to these wonderful reports, it is found that solution-derived synthesis based on aqueous/nonaqueous (organic) solution chemical methods has triggered increasing interest and has become the mainstream route to obtaining large-scale nano/micro-structured photoanode materials. Accordingly, in this review, solution-derived synthesis methods for obtaining ZnO nanostructured photoanodes of DSSCs are mainly covered. Meanwhile, it will also demonstrate how the morphologies and synthesis routes of ZnO nanostructures, together with the fabrication techniques for ZnO photoanodes, significantly influence DSSC performance. A few classic paradigms that have been landmarks in the preparation of ZnO nanoparticles, and 1D or 2D nanostructures as the

photoanode, will firstly be reviewed in brief; then, focus is put upon the latest optimization or modification of these ZnO nanostructured photoanodes for achieving low-cost production, desirable conversion efficiency, and persistent performance stability in practical applications. Additionally, some novel structural configurations of ZnO photoanodes are going to be introduced.

2. Nonaqueous solution system

Early in the 1960s, several attempts to use ZnO in PEC solar cells were performed. Originally, single-crystalline ZnO electrodes sensitized by Rhodamine B and Rose Bengal were studied by Gerischer[64] and Tributsch[65] in 1968. Later on, inspired by the great breakthrough in the conversion efficiency of particulate nanocrystalline TiO_2 photoanodes, ZnO nanoparticulate films were also introduced in DSSCs. These nanometer-sized particles are generally derived from the sol–gel method. Typically, an ethanolic solution of zinc acetate is heated in order to prepare an intermediate ZnO sol through hydrolysis and condensation. Then, nanostructured films are prepared by applying the sol to a conducting glass substrate to obtain solid wet gels by spin-coating or dip-coating methods.[66–68] Upon a post-thermal treatment, the gel is heated to form a porously structured ZnO film on the substrate. The doctor-blade method[69,70] and the screen-printing method,[71,72] initially developed for preparation of photoanodes of TiO_2-based DSSCs, have also been adopted to construct ZnO nanoparticulate films with the sol–gel-derived ZnO nanoparticles as the building blocks. However, these film preparation methods based on liquid-phase intermediate species unavoidably introduce some organic additives, and thus a subsequent heat-treatment is necessary, which could result in the crazing of nanoparticulate films and preclude the utilization of flexible plastic substrates that do not endure high heat-treatment temperatures. In this regard, A. Hagfeldt *et al.*[73,74] presented a new static film compression method to construct the photoanode film by mechanically compressing the sol–gel-derived ZnO nanoparticles under a pressure of 1000 kg cm^{-2} at room temperature. This new method for manufacturing nanostructured electrodes means an additional heat-treatment is not required since no organic additives are present in the film. Simultaneously, a better electrical contact between nanoparticles is achieved by the compression, decreasing the carrier recombination loss due to the reduced interparticle hopping steps during the charge-transport process within the photoanode. A typical scanning electron microscope (SEM) image of a ZnO nanoparticulate electrode with an average particle size of 150 nm, prepared in this way, is shown in Fig. 2(a). When the as-obtained nanoparticulate film acted as a photoanode in DSSCs, a comparatively high overall efficiency of 5% was attained by measuring the *I–V* characteristics of the DSSC with a 14 μm-thick ZnO photoanode, corresponding to Fig. 2 (b). According to the explanation by A. Hagfeldt *et al.*, utilization of the compression method without introducing organic additives during the film preparation led to better interfacial kinetics that should be responsible for the improvement in the conversion efficiency. Note that during their work, the employed illumination intensity of the cell testing was 10 mW cm^{-2}, which is one tenth of the standard intensity of 100 mW cm^{-2} conventionally used elsewhere. A weaker illumination may result in slightly higher conversion efficiency.[45] Moreover, the static mechanical compression method seems to be more appropriate for flexible substrates, which limits the adoption of rigid or frangible substrates in large-scale and continuous photoanode production, let alone their utilization in dynamic mechanical compression methods based on a roller mill with two cooperative rollers.[75]

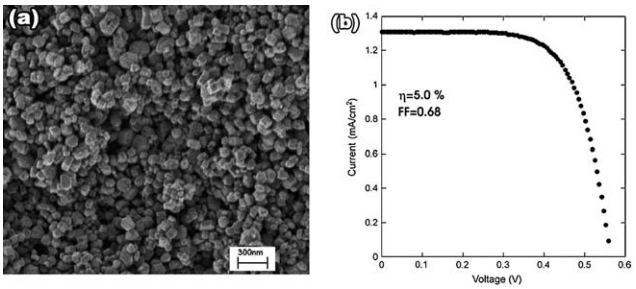

Fig. 2 (a) SEM image of a nanoparticulate ZnO film photoanode prepared by the compression method. The average particle size is 150 nm. (b) *I–V* characteristics of the DSSC with a 14 μm-thick ZnO electrode corresponding to (a).[74]

At present, the sol–gel method is still a frequently studied film-fabrication technique for constructing photoanodes.[76–78] For instance, M. F. Hossain *et al.*[79] and S. Rani *et al.*[80] systematically studied the effect of zinc concentration and pH value of the as-synthesized sol on the film morphology and the resultant cell conversion efficiency, respectively. M. C. Kao *et al.*[81] intensively investigated the effect of thermal treatment of the gel films on the cell performance. In their case, the gel films were annealed at 600 °C at different annealing rates of 5 °C min^{-1} and 600 °C min^{-1}, respectively. Results showed that rapid thermal annealing resulted in the formation of ZnO nanocrystalline films with better crystallization and higher porosity. DSSC characterization indicated that open-circuit and short-circuit photocurrent increased from 0.55 V and 4.38 mA cm^{-2} for the DSSC with slow thermal annealing derived films to 0.61 V and 5.88 mA cm^{-2}, respectively, for the DSSC with rapid thermal annealing derived films. Furthermore, M. C. Kao *et al.*[82] demonstrated that before the thermal annealing of gel films, different pre-annealing temperatures (100 °C and 300 °C) greatly influenced pore size and surface area of ZnO nanoparticulate films, as shown in Fig. 3. The increase in pore size and surface area with the increased pre-annealing temperature caused an improvement of the adsorption of N3 dye onto the films, the short-circuit

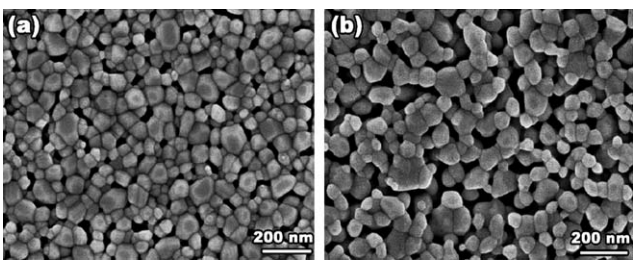

Fig. 3 SEM images of sol–gel-derived nanoparticulate films annealed at 600 °C with different pre-annealing temperatures: (a) 100 °C and (b) 300 °C.[82]

photocurrent, and the open-circuit photovoltage of DSSCs. A higher efficiency of 2.5% with the short-circuit photocurrent and an open-circuit photovoltage of 8.2 mA cm^{-2} and 0.64 V, respectively, was obtained for the ZnO nanocrystalline film pre-annealed at 300 °C. More recently, the sol–gel method was further modified and aerogel templated ZnO nanocrystalline films, with a typical size of 8.4 nm, were achieved by T. W. Hamann *et al.*[83] Using the aerogel-template derived ZnO nanoparticulate films to act as the photoanode, a 2.4% conversion efficiency was obtained.

With the main intention of achieving a large surface area for loading more dye photosensitizers and absorbing more incident light, the sol–gel-derived ZnO nanoparticles are used as photoanodes of DSSCs. However, some exterior factors were frequently neglected. For instance, if the incident light is utilized more effectively, the cell performances should have more space to increase further, without needing laborious enhancement in the surface area. Alternatively, an effective method to enhance the efficiency in DSSCs is to build a light scattering layer with enhanced photo-capture efficiency and optical absorption within the photoanode films.[84–86] Following this strategy, submicrometer/micrometer-scale particles in the photoelectrode have been employed as light scattering centers based on the fact that optical absorption has been enhanced to a large extent when TiO_2 nanocrystalline films were combined with larger particles.[87–90] Many researchers have succeeded in improving the conversion efficiency of TiO_2-based DSSCs by admixing large-sized SiO_2, Al_2O_3, or TiO_2 as light-scatterers.[91–94] However, the introduction of large-sized particles into nanocrystalline films unavoidably lowers the internal surface area within the photoelectrode film. This could counteract the enhancement effect of light scattering on the optical absorption. In this regard, a sol–gel-derived ZnO hierarchically structured film with spherical aggregates comprised of closely packed ZnO nanocrystallites has also been recently introduced into the photoanode film by Q. F. Zhang and T. P. Chou *et al.*[95–97] It is expected that these ZnO aggregates with a submicrometer size that is comparable to the wavelengths of incident light can result in light scattering. As a result, the traveling distance of light is significantly extended by several hundred times, leading to an increase in the light-harvesting efficiency of the photoanode. The synthesis of spherical ZnO aggregates can be achieved by hydrolysis and condensation of zinc salt in a polyol medium, which is characteristic of the sol–gel process.[98–101] In a typical case,[96] zinc acetate dehydrate (0.01 mol) was added to diethylene glycol (DEG, 100 mL) and then was heated under reflux to 160 °C. By adjusting the heating rate during synthesis, or adding a stock solution containing 5-nm ZnO nanoparticles also prepared by a sol–gel approach, ZnO spherical aggregates with either a monodisperse or polydisperse size distributions can be prepared. The photoelectrode films were fabricated on FTO glass using a drop-cast method, as shown in Fig. 4(a). Fig. 4(b) shows the morphology of an individual ZnO spherical aggregate that is formed by numerous interconnected nanocrystallites, with sizes ranging from several tens to several hundreds of nanometers (Fig. 4(c)). Typically, for photoanodes constructed with such polydisperse ZnO spherical aggregates, a maximum short-circuit current density of 19 mA cm^{-2} and conversion efficiency of 5.4% are achieved.[96] In this case, the authors thought that the performance of the solar cell was

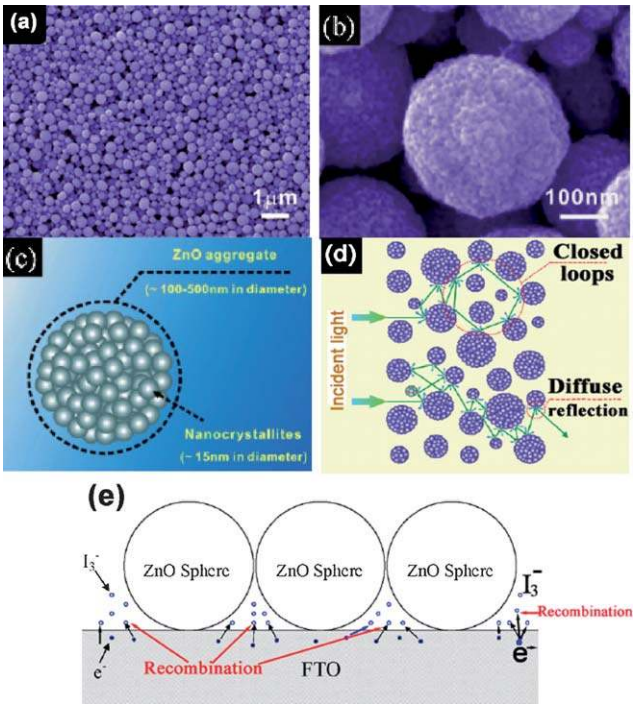

Fig. 4 (a) An SEM image of ZnO hierarchical spherical aggregates composing a photoanode film. (b) An SEM image and (c) the schematic diagram of an individual ZnO hierarchical spherical aggregate comprised of closely packed ZnO nanocrystallites. (d) A schematic drawing of light scattering and photon localization within a film consisting of ZnO hierarchical spherical aggregates,[96] and (e) a schematic drawing of recombination occurring between the FTO substrate and the electrolyte.[103]

improved due to the presence of light scattering within the hierarchically structured ZnO films, by which the travelling distance of light within the photoelectrode film can be significantly extended. As such, the opportunities for incident photons to be captured by the dye molecules are increased. A photon-localization effect may also occur on these films due to their highly disordered structure that confines the light scattering in closed loops, as shown in Fig. 4(d). Meanwhile, the film with aggregates consisting of interconnected nanosized crystallites provides a highly porous structure, ensuring a large specific surface area for dye adsorption, unlike the introduction of the large-sized particles that consume the internal surface area. Since then, it has become usual practice to apply ZnO films constructed with spherical aggregates assembled by nanocrystallites to the DSSCs, and similar works have been reported by many researchers, such as H. M. Cheng *et al.*,[102] Y. Z. Zhang *et al.*,[103,104] and J. C. Tao *et al.*[105] Among them, by optimization of dye photosensitizers, Cheng *et al.* also gained a comparatively high conversion efficiency of 5.34% under AM1.5 full sunlight illumination (100 mW cm^{-2}). After studying such hierarchically structured spherical aggregate photoanodes, Y. Z. Zhang *et al.* found that due to the spherical structure, most of the substrate surface is exposed to the electrolyte, and the recombination probability between the electrons, having been transferred to the substrate and the I_3^- in the electrolyte, could be strongly enhanced. A schematic drawing of this recombination is shown in Fig. 4(e).[103] To suppress this undesirable recombination, Zhang *et al.* pre-prepared a ZnO blocking layer of about 100 nm

by spin-coating sol–gel containing zinc salt to separate the FTO substrate and the electrolyte. Therefore, a great improvement in conversion efficiency was observed as a result of the decrease in the recombination.

3. Aqueous solution systems

3.1. Hydrothermal synthesis

Aside from the sol–gel derived ZnO nanoparticles, the hydrothermal (HT) method is also frequently used to synthesize ZnO nanoparticles. Strictly speaking, the hydrothermal synthesis should be defined as aqueous chemical synthesis reactions at temperatures of 100–1000 °C and under pressure of 1 MPa–1 GPa. Therefore, only those aqueous chemical syntheses of ZnO performed at above 100 °C in a sealed autoclave (Fig. 5) belong to the hydrothermal synthesis techniques. In a typical example given by A. E. Suliman *et al.*,[106] 13 g of $ZnCl_2$ and 8 g of NaOH was dissolved in distilled water, giving a white precipitate. Then, the precipitate was washed with the distilled water and mixed with 50 mL of PVP solution during continuous stirring to homogenize the solution. The homogeneous solution was transferred into an autoclave and heated at 160 °C for 8 h. Subsequently, the ZnO nanoparticulate powder was obtained (Fig. 6(a)) and dried at 100 °C after it had been washed with distilled water. Further, a second re-hydrothermal growth process could convert the hydrothermally synthesized ZnO nanoparticles into ZnO nanosheets *via* "oriented assembling" of the nanoparticles, as shown in Fig. 6(b). But, to transfer the hydrothermally grown ZnO samples onto the conducting substrate, they must be dispersed in ethanol to form a colloid, and then the colloid was applied onto TCO substrates by the conventional doctor-blade technique. Finally, 6 μm-thick crystalline ZnO films were formed by annealing at 450 °C. When both the ZnO films were sensitized by N3 dye and used as photoanodes in DSSCs, conversion efficiencies of 0.75% for the ZnO nanoparticle film and 1.55% for the ZnO nanosheet film were obtained. The authors thought that the difference in the conversion efficiency was related to the scattering of the incident light on the surface of both the photoanode films, because the two films have a different surface morphology. Besides the conventional film-preparation techniques, A. R. Rao *et al.*[107] recently reported the achievement of 4.7% conversion efficiency in ZnO DSSCs fabricated by spray-depositing hydrothermally synthesized nanoparticles. Spray deposition is well known for its simplicity and ease in controlling the spray parameters (*e.g.* solution flow rate, gas flow rate, concentration of the solution, and deposition temperature) in order to get the desired properties of the material.[108] Prior to preparing the films by this method, an organic solvent with better dispersion capacity is needed to disperse the hydrothermally synthesized ZnO nanoparticles so that the dispersed nanoparticles can be sprayed onto the desired substrates at a temperature just above the boiling point of the solvent. Importantly, the solvent used should evaporate easily during the deposition, which is crucial to the formation of the good quality ZnO nanocrystalline thin films on a substrate. 1-Butanol, which is well known for having advantageous dispersive properties due to its high viscosity and low boiling point (118 °C), is often used as the solvent for the dispersion of ZnO nanoparticles. In A. R. Rao's case, the films were deposited on quartz and FTO (SnO_2:F) substrates kept at 200 °C by applying different voltage. Significantly, this technique for preparation of the ZnO photoanode has been transplanted to the synthesis of TiO_2 films, attaining an overall conversion efficiency of about 5%.[109,110]

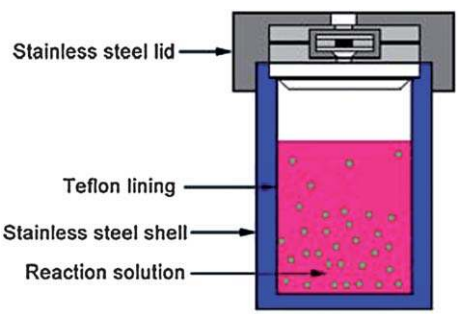

Fig. 5 Schematic diagram of a Teflon lined stainless steel autoclave for hydrothermal synthesis of ZnO.

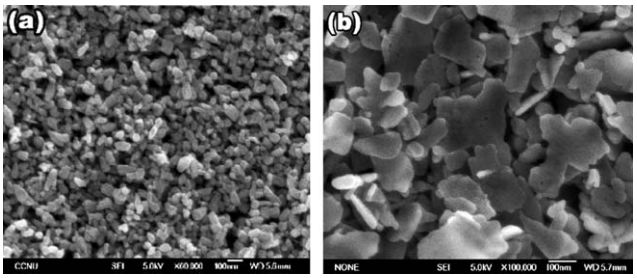

Fig. 6 SEM images of the hydrothermally grown (a) ZnO nanoparticles and (b) ZnO nanosheets.[106]

In the hydrothermal synthesis of ZnO nanostructures, some inorganic or organic substances are often added to the solution as the capping agent or the surfactant to obtain various ZnO nanostructures, such as rod-like, platelet-like, flower-like and sphere-like structures.[111–113] The capping agent or the surfactant can expedite or restrain the growth speed of different crystal planes, thus controlling and modifying the shape and morphology of hydrothermally grown products. For instance, M. S. Akhtar *et al.*[114] used a capping agent-assisted hydrothermal method to fabricate various ZnO nanostructured materials for use as photoanodes in DSSCs. In their case, three 100 mL aqueous solutions containing 2 g of $Zn(CH_3COO)_2$ were prepared, firstly. Then, 3 mL of ammonia solution (0.3 M), 1.0 g of citric acid and 1.0 g of oxalic acid were added, and 15 mL of 5 M NaOH solution was introduced to adjust pH range to 10–11. The above-prepared solutions were then transferred to a Teflon lined a stainless steel autoclave that was sealed and maintained at 160 °C for 12 h. Finally, ZnO nanostructures with the morphology of flowers, sheet-spheres and plates were obtained by centrifugation with capping agents of ammonia, citric acid and oxalic acid, respectively, as shown in Fig. 7. When the three ZnO products were sensitized by N719 dye and used as the photoanodes of DSSCs, a highest conversion efficiency of 2.6% was obtained for the DSSC fabricated with sheet-sphere ZnO nanostructures (Fig. 7(b)). The authors concluded that the photoanode with the ZnO sheet-spheres prepared using citric

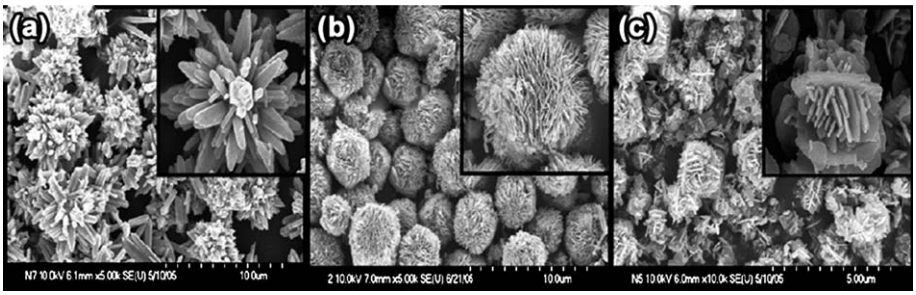

Fig. 7 SEM images of ZnO nanostructures with the morphology of (a) flowers, (b) sheet-spheres and (c) plates that were hydrothermally grown with capping agents of ammonia, citric acid and oxalic acid, respectively.[114]

acid as the capping agent had the highest internal surface area, which is beneficial for the dye absorption, resulting in an improved conversion efficiency. Also, the improved cell performance is also believed to profit from the high degree of crystallinity of the ZnO sheet-spheres, which leads to less resistance during the electron transfer.

Cetyltriethylammnonium bromide (CTAB) is a frequently used cationic surfactant in the hydrothermal synthesis of ZnO. In the CTAB-assisted hydrothermal synthesis of ZnO, using different starting materials can yield different ZnO nanostructures which greatly affect the resultant performance of DSCCs. In a typical case given by C. X. Wang *et al.*,[115] $Zn(NO_3)_2$ (a zinc salt) was used, and firstly dissolved along with NaOH in deionized water. Then CTAB was added into the solution and a white flocculent precipitate appeared immediately. Subsequently, the mixed solution was given a hydrothermal treatment at 120 °C for 24 h in a Teflon-lined stainless steel autoclave, and ZnO nanoflowers composed of nanorods were synthesized, as shown in Fig. 8(a). The surfactant generally reduces the surface tension of material. The surfactant CTAB can adsorb to the ZnO, resulting in self-assembling of ZnO nanorods into nanoflowers with assistance from the CTAB . In DSSC applications, the photoanode constructed from the ZnO nanoflowers exhibited a better degree of dye (N719) loading than that with ZnO nanorods prepared without adding CTAB in the same hydrothermal condition. Accordingly, a higher conversion efficiency of 1.37% was obtained for the ZnO nanoflower-based DSSC. In another CTAB-assisted case,[116] $Zn(CHCOO)_2$ and urea acted as the starting materials, and the hydrothermal synthesis was performed at 130 °C for 10 h in a Teflon-lined stainless steel autoclave. By pyrolyzing the hydrothermally grown plate-like hydrozincite ($Zn_5(CO_3)_2(OH)_6$) precursor, porous single-crystalline ZnO nanoplates were produced (see Fig. 8(b)). When the

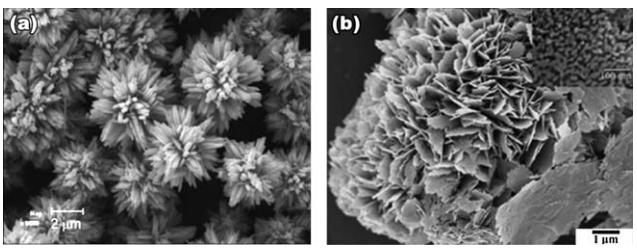

Fig. 8 SEM images of the hydrothermally grown (a) ZnO nanoflowers with $Zn(NO_3)_2$ and NaOH as the starting materials,[115] and (b) ZnO nanoplates with $Zn(CH_3COO)_2$ and urea as the starting materials.[116]

ZnO nanoplate photoanodes fabricated by the doctor-blade method were sensitized with N719 dye and integrated into the DSSCs, a comparatively high conversion efficiency of 5.05% was achieved. According to the authors' clarification, the enhanced conversion efficiency was most likely a result of enhanced light harvesting due to increased dye loading and effective light reflection and scattering of the photoanodes, as well as improved charge collection due to increased electron lifetime. This indicates that porous single-crystalline ZnO nanoplates can be a viable candidate for the development of highly efficient DSSCs.

The hydrothermal method cannot only be used to synthesize various pure ZnO nanostructures, but also it is an effective route to achieving facile modification of ZnO nanostructures using other functional materials. Hydrothermal synthetic integration of Au nanoparticles onto ZnO nanoflowers is a case in point.[117] The flower-like ZnO–Au nanocomposite was fabricated as follows: 2 mL of 0.1 M aqueous $HauCl_4$ solution was introduced into the previously mixed solution of 150 mL of 0.01 M aqueous $Zn(CH_3COO)_2$ solution and 6 mL of 6.67 M aqueous NaOH solution. Then, the newly mixed solution was immediately transferred into a Teflon lined stainless autoclave that was sealed and maintained at 180 °C for 2 h. After the complete reaction a pink colored solid powder was collected by centrifugation, followed by washing with distilled water and ethanol. SEM characterization shows the formation of ZnO nanoflowers decorated with Au nanoparticles (Fig. 9(a)) and the TEM image clearly shows that the petals of nanoflowers are dressed with several tiny Au nanoparticles of 10 nm in size (Fig. 9(b)). The high-resolution TEM image of the ZnO nanoflowers loaded with Au nanoparticles is shown in Fig. 9(c), and the high contrast difference between ZnO and Au is apparent. An interplanar distance of 2.46 Å corresponds to the (101) planes of ZnO and that of 2.33 Å corresponds to the Au (111) planes. All these prove the feasibility of modifying ZnO nanostructures with other functional materials using a facile one-pot hydrothermal synthesis. The DSSC based on the ZnO nanoflowers with Au nanoparticles sensitized by N3 dye shows a conversion efficiency of 2.5%, which is considerably higher than 1.6% of ZnO nanoflowers without Au nanoparticles. According to the authors' elucidation, the incorporation of Au nanoparticles into ZnO nanoflowers decreases the recombination centers generally attributed to the oxygen vacancies in ZnO, possibly by electron abstraction from the defects through the reduction of Au^+ ions, which leads to the great improvement in the cell performance.

Furthermore, the doping of ZnO by metal ions, such as Sn, Sb, In and so forth, can be readily carried out by the hydrothermal

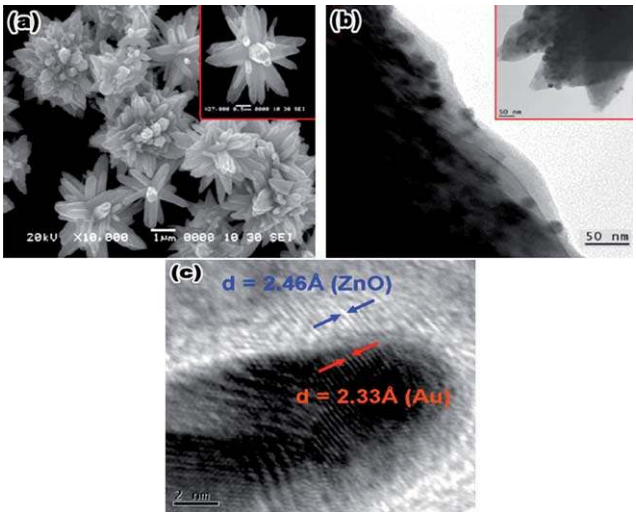

Fig. 9 (a) SEM, (b) TEM, and (c) high-resolution TEM images of ZnO nanoflowers with Au nanoparticles.[117]

synthesis. Very recently, N. Ye *et al.*[118] successfully used Sn-doped ZnO nanoparticles as photoanodes in DSSCs, and a gigantic enhancement in the conversion efficiency of DSSCs was achieved as compared to undoped ZnO nanoparticle-based DSSCs. The Sn-doped ZnO nanoparticles were hydrothermally synthesized using $ZnCl_2$, $SnCl_4$, PEG (polyethylene glycol 400) and NaOH. In brief, $ZnCl_2$ and $SnCl_4$, with a certain molar ratio, were dissolved in 100 mL deionized water. Then 25 mL of PEG 400 was slowly added into the solution. The pH of the mixed solution was adjusted to 12 by adding 2 M NaOH aqueous solution, whereafter the mixed solution was transferred into an autoclave and heated at 160 °C for 5 h. The undoped ZnO samples were also synthesized in the same hydrothermal conditions without the introduction of tin salt. DSSCs with 5.5% Sn-doped and undoped ZnO nanoparticulate films sensitized by N719 dye were assembled and the comparison of photovoltaic properties is presented in Table. 1. It can be seen that the I_{sc} and the V_{oc} for the DSSC constructed using the 5.5% Sn-doped ZnO films (I_{sc} = 9.18 mA cm^{-2} and V_{oc} = 0.64 V) show obvious improvement over the DSSC constructed using the undoped ZnO films (I_{sc} = 4.55 mA cm^{-2} and V_{oc} = 0.58 V). As is known, doping ZnO with Sn is a kind of n-type doping, which leads to an increase of charge carrier density and the rising of Fermi energy levels. As a consequence, the electron transport capacity of the ZnO was enhanced, and thus the higher I_{sc} was obtained. A higher I_{sc} would result in a higher η, since the η is partly dependent on the I_{sc}. Therefore, due to improved I_{sc} and V_{oc}, the Sn-doped ZnO nanoparticle-based DSSC attained a total power conversion efficiency of 3.79%, which is considerably superior to that of the undoped ZnO sample based DSSC (1.62%).

Table 1 The comparison of the photovoltaic properties of DSSCs fabricated with Sn-doped and undoped ZnO nanoparticles[118]

Sample	I_{sc}/mA cm^{-2}	V_{oc}/V	FF	η (%)
Undoped	4.55	0.581	0.62	1.62
5.5% Sn-doped	9.18	0.641	0.65	3.79

As with the above-mentioned ZnO nanostructures synthesized by hydrothermal methods, additional film-fabrication techniques such as the doctor-blade method or the screen printing method are often needed to construct the photoanodes of DSSCs. Also, the photoanodes ultimately work in the form of unordered nanostructured films during the electron transport. The excess electron hopping or scattering through the nanostructure units could result in a long dwell time, and thus increase the probability of electron recombination between the injected electrons and the oxidized dye or redox couple in the electrolyte. Therefore, a highly (110)-oriented ZnO porous nanosheet framework on an FTO (F:SnO_2) conducting glass substrates is designed as the photoanode in DSSCs.[119] ZnO nanosheet films were directly fabricated on FTO substrates *via* a hydrothermal precursor template method in a Teflon-lined stainless steel autoclave with $Zn(NO_3)_2$ and urea as the starting materials. FTO substrates were obliquely immersed into the reaction solution. After the hydrothermal reaction at 120 °C for 3 h, the precursor of hydrozincite ($Zn_5(CO_3)_2(OH)_6$) nanosheets were synthesized. By calcining the precursor, vertically aligned porous ZnO nanosheet arrays were successfully produced on FTO substrates, as shown in Fig. 10. The FTO substrate-assisted hydrothermal synthesis of ZnO nanostructures can be used to directly construct dense ZnO photoanode films (Fig. 10(a)), avoiding additional film-fabrication procedures. Fig. 10(b) and (c) clearly show the characteristic of porosity and vertical growth of the ZnO nanosheets, which is favorable for adsorbing more dye photosensitizers, and rapid electron transport and gathering within the photoanode film. As for the ZnO nanosheet framework, the (002) planes are perpendicular to the FTO substrate and (110) planes are parallel to it. According to the scanning tunnelling spectroscopy study of the electronic structure of the ZnO (001)-Zn, (00$\bar{1}$)-O, (100), and (110) surfaces, the (00$\bar{1}$)-O surface exhibits a higher conductance compared to the other surfaces.[120] Therefore, when the photogenerated electrons diffuse in the films, the (00$\bar{1}$)-O lattice planes of the nanosheets, which are upright on the substrate, work just like conducting wires and induce the electrons to transport to the

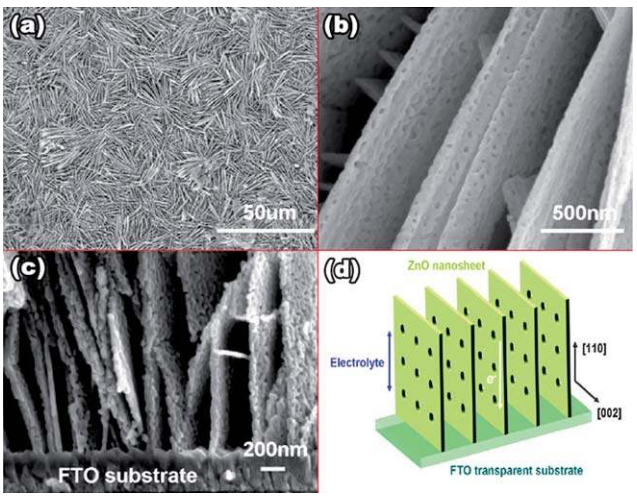

Fig. 10 ZnO porous nanosheet arrays synthesized by the hydrothermal method: (a) Low- and (b) high-magnification SEM images, (c) cross-section SEM images of ZnO nanosheet arrays, and (d) a schematic diagram of the ZnO porous nanosheet arrays photoanode.[119]

substrate (see Fig. 10(d)), resulting in improved electron collection. Typically, when a 20 μm-thick highly (110)-oriented ZnO porous nanosheet array was introduced into DSSCs sensitized by N719 dye, an impressive conversion efficiency of 3.7% was obtained.

3.2. Aqueous chemical growth

Currently, many researchers have come to the common understanding that ZnO nanostructures with direct pathways for electron transport are advantageous in designing the configuration of the photoanode.[121–125] In those desirable nanostructures, such as oriented 1D ZnO nanostructured arrays, the electrons directly transfer from the location of injection to the collection electrode with less electron scattering. This is different from the situation of nanoparticulate films where the electrons take a random walk among the nanoparticles and undergo a large amount of scattering and collisions. Intensity modulated photovoltage and photocurrent spectroscopes performed by B. F. Alex *et al.*[126] further corroborated that photoanodes based on 1D ZnO nanostructured arrays exhibit dramatically faster electron transport compared to the ones assembled from colloidal nanoparticles. In this regard, ZnO nanowires with dendritic structures grown by metalorganic chemical vapor deposition (MOCVD) techniques were first introduced into the DSSCs by E. S. Aydil in 2004,[127,128] with the intention of providing both high surface areas to maximize dye absorption and efficient electron transport that directly delivers the electron to the collection electrode with less recombination. Early ZnO nanowire-based DSSCs reported 0.5–1.1% conversion efficiencies. However, more economical and convenient synthesis methods based on solution chemical systems should be developed to meet the requirement of directly constructing ZnO nanowire array-based photoanodes. Actually, early in 2001, a low-temperature aqueous chemical growth (ACG) method had just been developed by L. Vayssirers *et al.*[129] to fabricate highly oriented microrod arrays of ZnO from aqueous solution. Later on, L. Vayssirers *et al.* further developed the ACG method in their subsequent outstanding work.[130–132] The ACG method seems to resemble the hydrothermal method mentioned above. However, the ACG method does not need the high temperatures and pressures that are generally used in a sealed autoclave, only a simple heater and a beaker containing the growth solution are used, as shown in a schematic diagram of an experimental device for ZnO aqueous chemical growth (see Fig. 11). During the growth of ZnO by the ACG method, a seeded substrate previously coated with a layer of ZnO nanocrystallites was frequently used to induce the nucleation and growth of the ZnO nanocrystal arrays. Therefore, in a way, the ACG method could be a seedlayer-induced hydrothermal synthesis with low temperature and pressure.

Benefiting from the success of L. Vayssirers in growing ZnO nanowire arrays, ZnO nanowires prepared by the ACG method were also incorporated into DSSCs by E. S. Aydil in 2005, and a schematic diagram of the nanowire-based DSSCs is displayed in Fig. 12(a).[133] In this case, ZnO nanowires were grown on FTO conducting substrates that were seeded in advance by a thin film of ZnO nanoparticles with diameters ranging from 5 to 10 nm. A 125 mL solution of 0.01 M zinc acetate in methanol was added

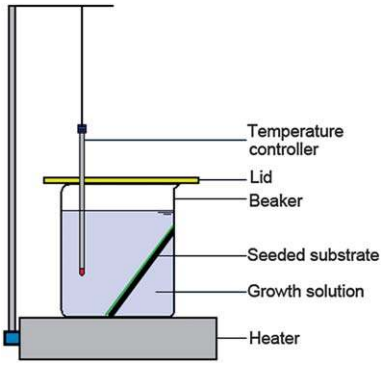

Fig. 11 Schematic diagram of an experimental device for ZnO aqueous chemical growth.

dropwise to a well-stirred 65 mL solution of 0.03 M NaOH in methanol maintained at 60 °C. After 2 h of growth, the solution was centrifuged to separate the nanoparticles. The supernatant was discarded and fresh methanol was infused to suspend the particles. The films (~100 nm) of nanoparticle seeds were then dispersed on FTO substrates by drop coating. Subsequently, ZnO nanowires were grown by the ACG method on the seeded substrates by placing them face-down in 0.025 M zinc nitrate and 0.025 M hexamethylenetetramine (HMT) aqueous solution at 60 °C. Nanowires were grown for 15 min to 4 h to study the evolution of the morphology as a function of growth time. Typically, the short-circuit current density of 1.3 mA cm^{-2} and overall power conversion efficiency of 0.3% were achieved with an 8-μm long nanowire film (Fig. 12(b)) sensitized by N719 dye. Notwithstanding this low conversion efficiency for DSSCs constructed with solution-phase processed ZnO nanowires, the ACG synthesis offers the potential for much lower production costs because it eliminates the expenses associated with high temperature manufacturing and vacuum processing. In addition, the ACG processing is easily scalable to large areas and is compatible with roll-to-roll processing of plastic substrates.

In order to further enhance the cell conversion efficiency, longer or ultralong nanowires produced by the ACG method were desirable in order to adsorb more dye photosensitizer molecules. Recently, it has been found that the introduction of polyethylenimine (PEI) into the growth solution as an additive could efficiently increase the length of ZnO nanowire arrays. In this regard, M. Law *et al.*[35] gave us a classic paradigm, achieving the longest arrays of 20–25 μm with a nanowire diameter that varied from 130 to 200 nm. Similar to L. Vayssirers's strategy,[130–132]

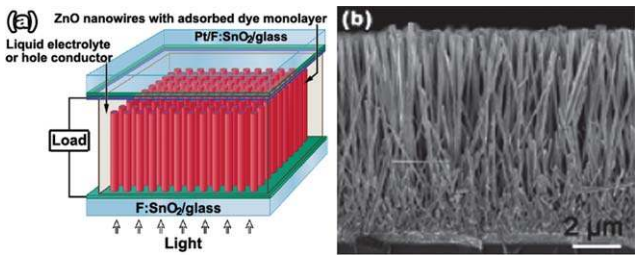

Fig. 12 (a) Schematic diagram of the nanowire-based dye-sensitized solar cell, and (b) the corresponding ZnO nanowire arrays.[133]

M. Law *et al.* also employed a thin film of ZnO quantum dots (dot diameter = 3–4 nm, film thickness = 10–15 nm) deposited on the FTO substrates *via* dip coating in a concentrated ethanol solution to induce the growth of ZnO nanowires in aqueous solutions containing 25 mM $Zn(NO_3)_2$, 25 mM HMT, and 5–7 mM PEI at 95 °C. Dissimilarly, after this period, the substrates were repeatedly immersed into fresh solutions for maintaining continuous ACG processes until the expected nanowire length was reached. At a full sun intensity of 100 mW cm^{-2} (AM1.5), the N719 sensitized DSSCs with the longest nanowire arrays of 20–25 μm were characterized by short-circuit current densities of 5.3–5.85 mA cm^{-2}, open-circuit voltages of 610–710 mV, fill factors of 0.36–0.38, and overall conversion efficiencies of 1.2–1.5%.

More recently, a modified ACG method for the preferential growth of ultralong ZnO nanowire arrays has been developed by C. K. Xu *et al.*[134] Their key idea for growing ultralong ZnO nanowires on seeded substrates is to suppress homogeneous nucleation while maintaining the growth of pre-existing ZnO nanocrystalline nuclei on seeded substrates. Considering that homogeneous nucleation is favored by a high degree of supersaturation, it is expected that moderately decreasing the degree of supersaturation would not significantly affect the growth rate of ZnO nanowires on the seeded substrates while suppressing formation of ZnO particles in the bulk solution. Likewise, a growth solution consisting of $Zn(NO_3)_2$ and HMT is adopted too. By introducing ammonium hydroxide to form complexes with the zinc ions that serve as a buffer for Zn^{2+} and continuously supply Zn^{2+} ions, a low degree of supersaturation of the reaction system can be obtained. However, a high concentration of ammonium hydroxide could also result in very slow growth of the nanowires on the seeded substrate, due to an excessively low degree of supersaturation. Therefore, PEI was simultaneously used along with ammonium hydroxide. It is thought that PEI can adsorb on the lateral planes of the ZnO nanowires by electrostatic attraction, allowing the development of a large aspect ratio. In the presence of both PEI and ammonium hydroxide, the formation of ZnO in the bulk solution can be effectively prevented while ZnO wires still grow on the seeded substrate at a reasonably high growth rate. The significance of this discovery is that ZnO nanowires may now grow on seeded substrates, without precipitation in the bulk solution, at a reasonable degree of supersaturation through the coordinated use of ammonium hydroxide and PEI. Because of the high growth rate and low sample contamination, this method is particularly useful for growing ultralong ZnO nanowires. By introducing the substrates into fresh growth solution baths every 3.5 h, arrays of ZnO nanowires up to 33 μm were readily synthesized, as shown in Fig. 13(a)–(e). The *I–V* curves of the DSSCs made with ZnO nanowire arrays with various lengths (11–33 μm) are presented in Fig. 13(f), indicating that the power conversion efficiency gradually increases as a function of the wire length, and reaches 2.1% as the film thickness increases to 33 μm.

Repeated growth can obtain desirable lengths of ZnO nanowires and has been adopted by many researchers,[135–137] even in the hydrothermal synthesis which needs a closed autoclave, the time-consuming repeated growth of ZnO nanowire arrays on ZnO seeded substrates was often performed for improved nanowire-based photoanodes.[138] However, the repeated introduction of fresh solution not only increases the fabrication cost,

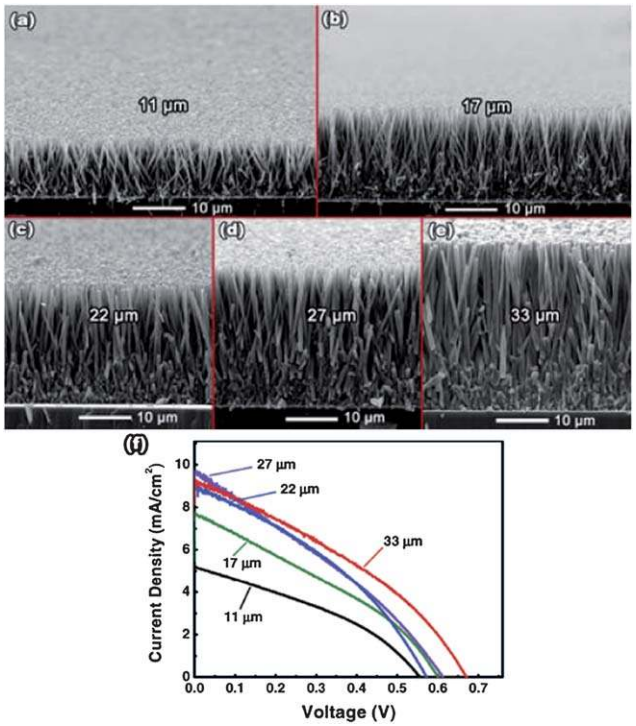

Fig. 13 SEM images of ZnO nanowire arrays of various lengths: (a) 11 μm, (b) 17 μm, (c) 22 μm, (d) 27 μm, and (e) 33 μm. (f) *I–V* characteristics of the DSSCs based on ZnO nanowire arrays with various lengths corresponding to (a)–(e).[134]

but also decreases the reproducibility. Therefore, a pre-heating PEI-assisted ACG method was developed by J. J. Qiu *et al.*[139] to fabricate longer ZnO nanowire arrays with high reproducibility. Typically, the growth solution was first sealed in a glass bottle and then heated to 95 °C for 2–12 h, which was a pre-heating process. Afterwards, the ZnO seeded substrates were quickly immersed in the hot pre-heated growth solution for the ACG process, which can keep the ZnO seedlayer on substrates from being destroyed by fresh growth solution in the initial growth stage. On the other hand, the original growth solution can be used until the whole growth process is over, which greatly decreases the fabrication cost. As a result, well-aligned ZnO nanowire arrays with a length of more than 40 μm were prepared successfully, and the DSSC performance based on the ultralong ZnO nanowire arrays sensitized by N719 dye was improved markedly.

During the practical operation of ZnO DSSCs, electron recombination between the injected electrons and oxidized dye or redox couple in the electrolyte is relatively serious. Particularly, electron recombination occurs across the conducting substrate–electrolyte interface, resulting in the poor cell performance. Therefore, a blocking layer is generally placed between the conducting substrate and ZnO nanostructures to effectively avoid contact of the conducting substrate and the electrolyte. For the growth of ZnO nanowires by the ACG method, Y. Q. Wang *et al.*[140] used a layer of TiO_2 nanoparticles as the blocking layer. Here, ZnO nanowire arrays were grown on the ZnO nanocrystalline seedlayer/TiO_2 nanoparticulate film/FTO/glass substrate (see Fig. 14(a)). Due to the suppression of interfacial

recombination by TiO_2 blocking layer, a higher conversion efficiency of 2.15% was attained for the DSSC with the blocking layer, schematically illustrated in Fig. 14(b), as compared to 1.46% for the one without the blocking layer. The improved cell performance was also characterized by a low dark current, which is mainly caused by electron recombination between the photoinjected electrons and positively charged dye molecules and electrolyte. Recently, ZnO nanowire-based DSSCs without the conducting substrate have been exploited by M. H. Lai *et al.*[141] in order to improve electron transfer by virtue of eliminating the electron scattering that generally derives from the heterogeneous interface between the conducting substrate and ZnO. The conducting substrate-free structure consists of ZnO nanowire arrays grown on a ZnO thin film on ordinary glass substrates by a two-step ACG method. The ZnO thin film replaced frequently used FTO to act as the conducting substrate. It is demonstrated that the conducting substrate-free DSSCs can operate properly, like the DSSCs with the conducting substrate. A subsequent study on the conducting substrate-free ZnO DSSCs from S. H. Lee *et al.*[142] has even showed that ZnO nanowire arrays grown by the ACG method on the Al-doped ZnO (AZO) thin films exhibited a better cell performance than those fabricated on the FTO conducting substrates. This is due to the facilitated charge injection from ZnO nanowires to the AZO films, resulting from the formation of an ohmic contact. The small difference in the work function between ZnO (5.1–5.3 eV) and FTO (4.9 eV) does not provide sufficient driving force for the injection from ZnO nanowires to FTO, while AZO films with a reported work function of 3.7–4.6 eV can meet the requirement. This study demonstrates that AZO films are more favorable for highly efficient ZnO nanowire-based photoenergy conversion devices. Moreover, similar to M. H. Lai *et al.* and S. H. Lee *et al.*, ZnO nanotips/Ga-doped ZnO films obtained by two-step metal–organic chemical vapor deposition (MOCVD) were also applied in the conducting substrate-free DSSCs by H. H. Chen *et al.*[143–145]

Electrochemical test techniques are used to evaluate the DSSCs with 1D ZnO nanostructured arrays prepared by the ACG method. Electrochemical impedance spectroscopy (EIS) has been shown to be effective for studying the electron transport and recombination properties of ZnO nanorod-based DSSCs. After carrying out EIS characterization on these DSSCs, C. He *et al.*[146] revealed that the recombination process in the cell is mediated by an exponential distribution of surface trap states on the rods, and this is shown to be a major efficiency-limiting factor for this type of device. In this respect, the electron recombination in ZnO nanowire/rod DSSCs can be effectively suppressed and the conversion efficiency enhanced by coating the nanowires/rods in a conformal metal oxide shell. Over the past few years, many researchers have described the effects of overcoating nanocrystalline TiO_2 or SnO_2 films in thin layers (1–30 Å) of insulating or semiconducting oxides, including Nb_2O_5, Al_2O_3, MgO, $SrTiO_3$, SiO_2, Y_2O_3, ZrO_2, SnO_2, and TiO_2.[78, 147–150] For example, M. Law *et al.*[151] applied 10–25 nm-thick TiO_2 shells on ZnO nanowire arrays grown by the ACG method, which caused a dramatic increase in V_{oc} and fill factor. This resulted in a substantial improvement in the overall conversion efficiency of up to 2.25%, which is superior to 1.2–1.5% of naked ZnO nanowire-based DSSCs previously made by M. Law *et al.* and his coworkers.[35] In principle, an oxide shell can suppress recombination by (i) introducing an energy barrier that increases the physical separation between photoinjected electrons and the oxidized redox species in the electrolyte, (ii) forming a tunneling barrier that corrals electrons within the conducting cores of the nanoparticle film, or (iii) passivating recombination centers on the oxide surface. A lower rate of recombination appears as a smaller dark current (I_{dark}), which can increase the open-circuit voltage (and fill factor) of a DSSC. Whether I_{sc} and cell efficiency also improve depends on the extent to which the electron injection and collection yields are hurt by the oxide shell. In addition to suppressing recombination, a shell can raise cell V_{oc} directly if it has a more negative conduction band edge than the core oxide or if it creates a dipole at the core–shell interface that shifts the band edge of the core upwards in energy.[152] Moreover, EIS can also play an important role in singling out proper dye photosensitizers for DSSCs. It is well known that the strategy for studying ZnO-based DSSCs is almost the same as that adopted for TiO_2-based ones. It can be regarded as a straight implantation of TiO_2-based Grätzel-type solar-cell technology, in which TiO_2 is replaced by ZnO while the dye sensitizer and the electrolyte remain unchanged. Thus, dyes such as N3 and N719 and the electrolyte employed in the reported ZnO nanowire-based DSSCs, which are directly adopted from TiO_2-based DSSCs, may not be suitable for ZnO materials. It has been shown that the performance of ZnO-based DSSCs decreases with increasing concentration of N3 dye on the surface of the photoanodes, since the formation of aggregates (dye/Zn^{2+}) of N3 dyes with Zn^{2+} ions results in inefficient electron injection from the dye/Zn^{2+} aggregates to the ZnO photoanodes. In this regard, J. J. Wu *et al.*[153] further used EIS and open-circuit photovoltage decay (OCPD) measurements to compare the electron transport properties of N3 and mercurochrome sensitized ZnO nanowire-based DSSCs. EIS measurements reveal that the electron recombination resistance in the mercurochrome/ZnO nanowire DSSCs is larger than that in N3 sensitized cells. OCVD analyses show that N3 sensitized ZnO nanowire photoanodes possesses a higher surface trap density in comparison to the mercurochrome-sensitized ones. This indicates that more electron interfacial recombination occurs in the N3-sensitized ZnO nanowire DSSCs due to the higher surface trap density in the ZnO nanowire photoanodes after N3 dye adsorption. The investigation from J. J. Wu *et al.* proved the superiority of mercurochrome dye for application in ZnO-based DSSCs.

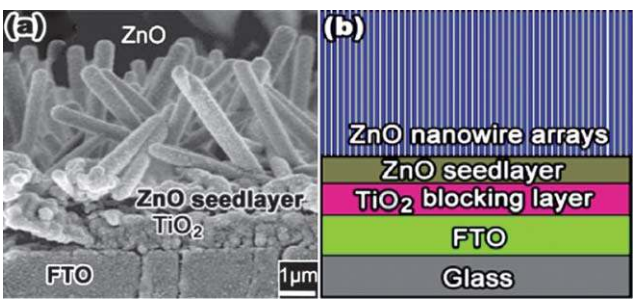

Fig. 14 (a) SEM image and (b) schematic diagram of ZnO nanowire arrays grown on the ZnO nanocrystalline seedlayer/TiO_2 nanoparticulate film/FTO/glass substrate.[140]

Besides ZnO nanowire arrays, another member of the family of 1D ZnO nanostructures, nanotube arrays, have also been successfully obtained by etching the ZnO nanowire arrays prepared by the ACG method. Due to their hollow tubular structures, ZnO nanotubes are expected to have a higher porosity and larger surface areas compared to ZnO nanowires/nanorods of the same sizes. Generally, ZnO nanotubes are indirectly made from pre-prepared ZnO nanorods/nanowires by preferential etching along the axial direction in acidic/basic solutions,[154–158] or in a system containing some aggressive substances such as Cl^- ions.[159] Even if one-pot synthesis methods were utilized to directly produce ZnO nanotubes, these two successive growth stages (firstly the formation of nanorods/nanowires and then the conversion of nanorods/nanowires into nanotubes) are actually indispensable. M. Guo *et al.*[160] have reported a 2.3% conversion efficiency of the DSSC based on ZnO nanotube arrays with average diameters of 500 nm and a density of 5.4×10^6 cm^{-2} (Fig. 15) that were prepared by a modified one-pot approach developed by L. Vayssieres *et al.*[129] Further increasing the surface area of ZnO nanotubes needs to produce longer nanotube arrays with larger aspect ratio. However, it is very difficult because the achievement of single-crystalline and vertically aligned arrays of ultralong nanotubes still remains a significant technological challenge in a solution-phase system. Therefore, to date, among all the ZnO nanotube-based DSSCs reported, satisfactory cell performances have not been achieved. With the help of lacunaris rigid templates, ultralong polycrystalline ZnO nanotubes (up to tens of microns) can also be fabricated by solution-phase or non-solution-phase synthesis techniques. Unfortunately, when these ultralong polycrystalline ZnO nanotube arrays were used to construct DSSCs a relatively low conversion efficiency of only 1.6% was achieved.[161]

Frankly speaking, although much effort has been directed towards the enhancement of electron transport in DSSCs using 1D ZnO nanostructures, so far none of these ordered ZnO 1D nanostructured DSSCs have achieved an efficiency that exceeds that of the conventional TiO_2 nanoparticle-based DSSCs. This is because that the improvement resulting from these ordered 1D nanostructured arrays is often offset or diminished by the deterioration in other device parameters intrinsically associated with the utilization of these 1D nanostructures, such as the two-sided effect of the length of the nanowires impacting the series resistance and roughness factor.[35] In this regard, Z. Z. Yang *et al.*[162] presented a new idea to mitigate this problem by allocating part of the roughness factor to the conductive substrate with 1D microtip arrays instead of imparting all the roughness factors onto the ZnO nanostructured films attached to the conductive substrate. They used microscopically rough Zn microtip arrays as the electron collecting substrate on which ZnO nanotips were grown by the ACG method to serve as the photoanode semiconductor component of the DSSC. Fabrication of the Zn-microtip|ZnO-nanotip composite nanoarchitecture can be described as follows.[163,164] A highly ordered array of Zn microtips can be obtained by anodizing the polished Zn foil in a freshly prepared NH_4Cl/H_2O_2 aqueous solution at a current density of 14 mA cm^{-2}, as shown in Fig. 16(a). Then, an ACG process was applied to grow ZnO nanotips on the Zn microtips (Fig. 16(b)). According to the TEM observation shown in Fig. 16(c), ZnO nanotips grew on the surface of the Zn microtips to about 300 nm in length. For the same surface roughness factor, the Zn-microtip|ZnO-nanotip DSSC (Fig. 16(d)) exhibited an enhanced fill factor compared with the DSSCs that have ZnO nanowires supported by a planar photoanode. In addition, the open-circuit voltage of the Zn-microtip|ZnO-nanotip DSSC is also improved due to a favorable band shift at the Zn–ZnO interface, which raises the Fermi level of the semiconductor and consequently enlarges the energy gap between the quasi-Fermi level of ZnO and the redox species. EIS studies reveal that the electron collection time is much shorter than the electron lifetime, suggesting that fast electron collection occurs in this reported device due to the significantly reduced electron collection distances along the short ZnO nanotips. Eventually, a moderate conversion efficiency of 1.4%, with an open-circuit voltage of 770 mV and a short-circuit current of 3.5 mA cm^{-2}, was obtained.[162]

As an alternative to the synthesis of 1D ZnO nanostructures that need a pre-prepared seedlayer on the conducting substrate to induce an ACG process, C. Y. Jiang *et al.*[165] directly synthesized branched ZnO nanoflower array films by immersing a clear FTO

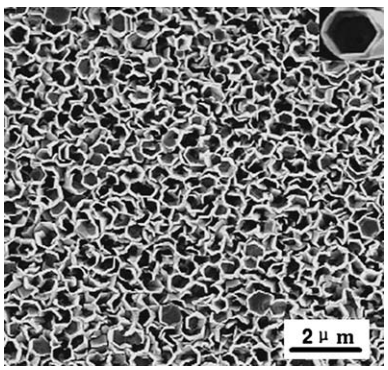

Fig. 15 A top view SEM image of ZnO nanotube arrays prepared by a modified one-pot ACG approach.[160]

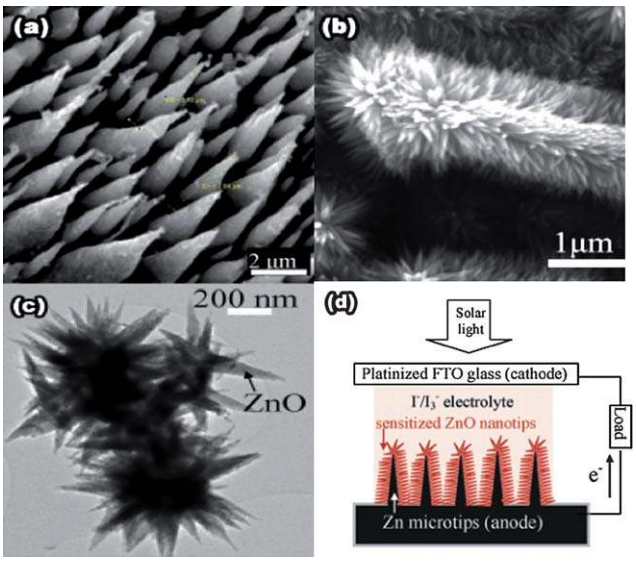

Fig. 16 Typical SEM images of (a) Zn microtips and (b) ZnO nanotips grown on Zn microtips, (c) TEM image of ZnO nanotips, and (d) a schematic diagram.[162]

substrate, without any surface modification, into a 0.005 M $ZnCl_2$ aqueous solution with a small amount of ammonia at 95 °C for 16 h. It can be seen from Fig. 17 that ZnO nanoflowers comprise of an upstanding nanorod crystal and several smaller nanorod crystals that randomly surround it. Theoretically, an upstanding nanorod array may be not favorable for light harvesting or light–dye interactions because some photons could fall into the gaps between adjacent ZnO nanorods, and be unable to undergo absorption by the dye interfacing ZnO. Even for the light shining vertically on the nanorods, the absorption is not complete because the light might only pass through one thin layer of dye-ZnO interface at the end of the rod. Therefore, the light loss may be significant for upstanding ZnO arrays. As for the nanoflower morphology in Fig. 17, the random branches of the nanoflowers provide both a larger surface area and increased light–dye interactions, whilst maintaining good electron transport. With this improvement in morphology, the branched ZnO nanoflower DSSC attained a power conversion efficiency of 1.9%, that is higher than the 1.0% for films of nanorod arrays with comparable diameters and array densities that were also fabricated by the ACG method. Furthermore, F. P. Yan *et al.*[166] elaborately studied the dye sensitization process of the ZnO nanoflower photoanode with N719 dye photosensitizer. They mainly focused on distinguishing the influence of dye-induced aggregation from that of dye-induced etching on the conversion efficiency. It is found that the dye-induced etching of the ZnO anode may result in the low efficiency of ZnO-based DSSCs. This is because the etching of ZnO may lead to a low surface absorption efficiency of the dye, low electron mobility, and a high surface recombination ratio of photocarriers. Therefore, we suggest that special attention should be paid to protecting the surface structure of the ZnO photoanodes during the dye-sensitizing process.

3.3. Chemical bath deposition

Chemical bath deposition (CBD), also known as controlled precipitation, electroless plating, or simply chemical deposition,[167] is frequently used for depositing different metal chalcogenide and oxide thin films from solution onto a substrate.[168] Typically, the CBD process is based on three chemical reactions steps:[169] (1) The formation or the dissociation of solvated ionic metal–ligand complexes, (2) hydrolysis of the complexes, and (3) the formation of solid phases. In cases where a complexing agent is used, the equilibrium between the agent and water should also be associated with step (1). The progress of step (2) produces less soluble chemical species and causes a low degree of supersaturation of the solutions, which results in heterogeneous nucleation on the foreign substrate in step (3). Originally, the CBD method was developed for ceramic thin-film formation on functionalized interfaces through biomimetic processing from aqueous solutions. Recently, CBD has been indirectly used to obtain ZnO films by pyrolysis of a ZnO intermediate precursor directly prepared by the CBD method. Generally, a precursor to ZnO was firstly synthesized and then it was converted into ZnO *via* solid-state crystal phase transformation upon a subsequent thermal treatment, without altering the original morphology.

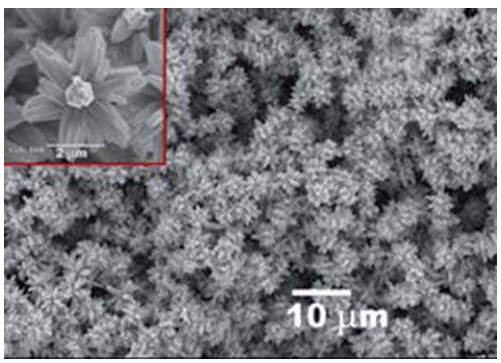

Fig. 17 SEM images of branched ZnO nanoflower arrays grown on FTO substrates by hydrothermal synthesis.[165]

Based on the CBD synthesis route, E. Hosono *et al.*[170,171] and K. Kakiuchi *et al.*[172,173] (from the same research team) pioneered the first fabrication of an upright-standing ZnO nanosheet array for use as a photoanode in DSSCs. A solution with a zinc concentration of 0.15 M for the CBD process was prepared by dissolving $Zn(NO_3)_2$ and $(NH_2)_2CO$ in water at room temperature. The weight ratio of $(NH_2)_2CO$: H_2O was 1 : 5. Borosilicate glass slides or FTO substrates were used as substrates for the deposition. The substrates were put into bottles filled with $Zn/(NH_2)_2CO$ solution, which were sealed and kept at 60 °C for 12–48 h. After the deposition, upright-standing layered hydroxide zinc carbonate (LHZC) sheets on the substrates were obtained[170–172] and then transformed into mesoporous ZnO nanosheet arrays by heating at 300 °C. Moreover, layered hydroxide zinc carbonate (LHZA) with the same sheet-like morphology as LHZC was also prepared and used as the precursor to ZnO.[173] In this case, a solution for the CBD process was prepared by dissolving $Zn(CH_3COO)_2 \cdot 2H_2O$ (0.15 M) in methanol. The DSSCs prepared using these upright-standing ZnO nanosheet films with 4 μm, 10 μm, and 20 μm in thickness exhibit conversion efficiencies of 3.3%,[172] 3.9%,[170] and 4.1%,[173] respectively, that correspond to the cases where the dye of N719 was used to sensitize the photoanodes. When the N719 dye was replaced with D149, further improvement to 4.27% in conversion efficiency was achieved for the 20 μm-thick photoanode DSSC.[171] It is worthy to note that D149 dye, as opposed N719 dye, is a metal-free indoline organic dye with outstanding performance. This is due to its high molecular extinction coefficient and its good compatibility with ZnO, which results in reduced complexing properties for zinc ions and suppresses the formation of aggregates (dye/Zn^{2+}). It is believed that these high conversion efficiencies were due to the specific morphology of upright-standing ZnO nanosheets, with the vertical intervals spanning from the substrate to the top of each sheet (Fig. 18(a)–(c)[172]). This allowed for an easy distribution and a rapid adsorption of the dye, thus preventing the formation of complex dye/Zn^{2+} aggregates. Even for a 20 μm-thick photoanode sensitized for a relatively long immersion time of 6 h, the cell performance was not degraded, indicating that aggregates of dyes can be avoided. Also, this kind of microstructure is expected to be beneficial for the electrolyte diffusion into the film, decreasing the resistance of the cell and the recombination of the injected electrons.[170] Further, TEM characterization (Fig. 18(d)[172]) shows that the ZnO nanosheet is composed of nanoparticles of approximately 20 nm in size along with

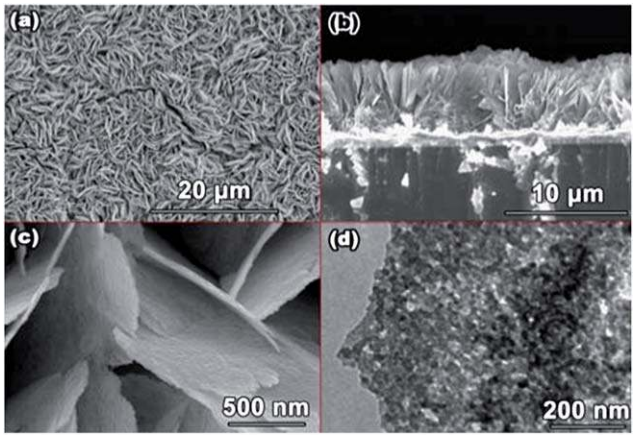

Fig. 18 (a) ZnO nanosheet arrays derived from CBD method: (1) Surface and (2) cross-section SEM images of ZnO nanosheet arrays, and (3) high-magnification SEM and (4) TEM image showing nanoparticles and mesoscopic pores among nanoparticles.[172]

mesoscopic pores among nanoparticles, which derived from the pyrolysis of LHZC or LHZA nanosheets prepared by the CBD method. The resultant films have larger surface areas than those of traditional films that are fabricated by controlling the crystal growth process of ZnO. This is because single-crystal ZnO has a small surface area due to flat surface at the atomic level. A larger surface area within the photoanodes will be helpful for adsorbing more dye molecules.

Furthermore, E. Hosono *et al.*[174] used the CBD method to directly fabricate ZnO films composed of hierarchical spherical aggregates with sheet-like crystals (Fig. 19) that have a strong light scattering enhancement effect. Precursor solutions for the CBD process were prepared by dissolving $Zn(CH_3COO)_2$ in methanol. FTO glass used as the substrate was immersed into 0.15 M precursor solutions for the deposition at 60 °C. It was demonstrated that the degree of light scattering may be a significant factor in determining the conversion efficiency in this case, and the DSSCs using the resultant ZnO films as the photoanodes exhibited a conversion efficiency of 2.0% under the AM-1.5 illumination at 100 mW cm^{-2}.

Aiming at further optimizing the performance of the vertically aligned ZnO nanosheet-based DSSCs, R. Zhang *et al.*[175] carried out studies on the adsorption of N3 dye onto sheet-like ZnO nanostructures grown by the CBD method. At lower dye concentrations of 0.05 mM, very little adsorption occurred in the first 30 min at 25 °C (Fig. 20(a)). With all the conditions the same, except an extension of the adsorption time to 44 h, the surface of ZnO film was covered with spherical aggregates with average diameters of 1 μm (Fig. 20(b)). Increasing the temperature to 40 °C reduced the formation of these aggregates on the surface of ZnO film (Fig. 20(c)). Increasing the dye concentration to 0.25 mM and keeping the temperature above 40 °C eliminated the formation of spherical aggregates. This was verified by the SEM images shown in Fig. 20(d). These results showed that dye adsorption was significantly influenced by dye concentration, immersion time and temperature. Temperature was determined to be a key factor in controlling dye adsorption and dye aggregation on the surface of ZnO films. Higher temperatures can increase the amount of dye adsorbed on ZnO. Moreover, higher temperature effectively reduce the occurrence of dye aggregation.

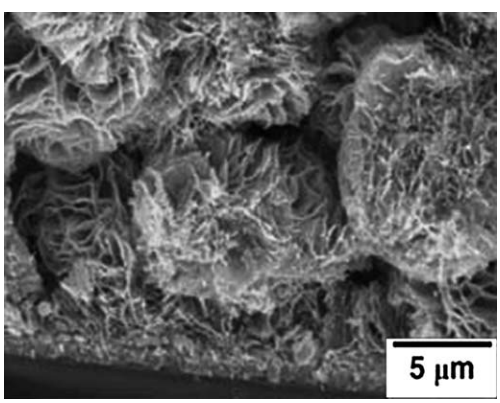

Fig. 19 SEM image of ZnO hierarchical spherical aggregates composed of sheet-like crystals prepared by CBD method.[174]

3.4. Electrodeposition

The electrochemical deposition (electrodeposition, ECD) technique is another potent means that can directly construct ZnO films on conducting substrates. Early in 1996, the ED of ZnO had been achieved simultaneously by M. Izaki *et al.*[176] and S. Peulon *et al.*,[177] using the same three-electrode electrochemical configuration (Fig. 21). Since then, the ECD of ZnO films has triggered considerable interest due to its distinctive advantages, such as the precise control over the film thickness and morphology, the possibility to prepare films with large area, relatively high deposition rate, low growth temperature, and low cost. The most important aspect in the ECD of ZnO is the reduction of an oxygen precursor at the interface of an electrode and a zinc salt solution, which controls the growth rate and affects the crystallinity and morphology of the obtained film significantly. M. Izaki *et al.*[176] used $Zn(NO_3)_2$ solution to act as both the zinc and oxygen precursor, while S. Peulon *et al.*[177] used a $ZnCl_2$ solution and dissolved molecular oxygen as the zinc and oxygen

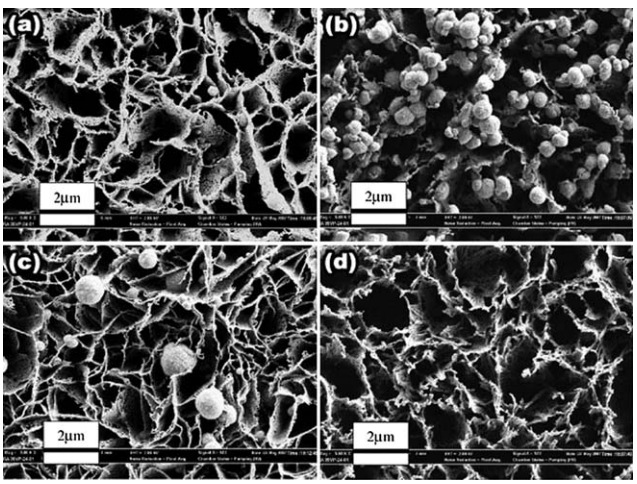

Fig. 20 SEM images of dye-adsorbed ZnO nanosheet photoanodes: (a) 0.05 mM, 0.5 h, and 25 °C; (b) 0.05 mM, 44 h, and 25 °C; (c) 0.05 mM, 44 h, and 40 °C; and (d) 0.25 mM, 44 h, and above 40 °C.[175]

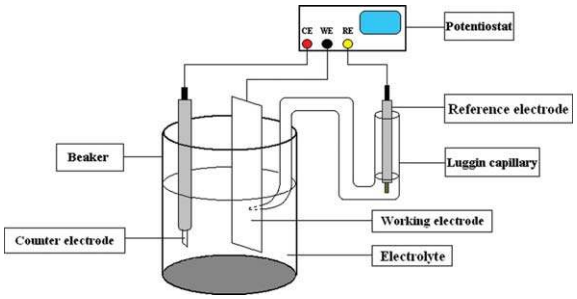

Fig. 21 Three-electrode electrochemical configuration for electrodepositing ZnO thin films.

precursor. It was demonstrated that by the optimization of appropriate deposition parameters, compact ZnO nanoparticulate films can be electrodeposited on metallic conducting substrates or FTO substrates.

Based on their successful ECD of ZnO nanoparticulate films, the researchers further modified the ECD conditions in order to achieve desirable film structures for use in DSSCs. For instance, Y. Y. Xia *et al.*[178] directly electrodeposited ZnO nanoparticulate films with porous nanostructures on an ITO substrate at a low temperature of 40 °C. The electrolyte used contained 0.04 M $Zn(NO_3)_2$ and 0.04 M HMT in a solvent with a mixture of distilled water and ethanol at a ratio of 1 : 1. The addition of ethanol as a wetting agent to the electrolyte solution may improve the thickness uniformity and surface coverage. It was demonstrated that applying a potential of −0.7 V resulted in the formation of ZnO nanoparticulate films. When the as-electrodeposited samples were used in DSSCs, a 1% power conversion efficiency was obtained. Moreover, poly(vinyl pyrrolidone) (PVP, MW ≈ 40 000) was also added to the electrolyte by Chen *et al.*[179] to control the morphology of electrodeposited ZnO nanoparticulate films. In their synthesis experiments, the ECD of ZnO nanoparticulate films was carried out at −1.1 V at 60 °C in the electrolyte containing 0.1 M $Zn(NO_3)_2$ and 0.1 M KNO_3 solution with the addition of 0–8 g L^{-1} PVP. The FTO substrate was used as the working electrode, with a pure zinc sheet as the counter electrode and a saturated calomel electrode (SCE) as the reference electrode. It was thought that PVP can coordinate with Zn^{2+} to tune the Zn^{2+} ion concentration in the electrolyte, thereby controlling reaction rate between Zn^{2+} ions and hydroxide ions. The nanoparticle size of ZnO films can be strongly influenced by the PVP concentration. Especially, the ZnO nanoparticulate film electrodeposited in the electrolyte containing 4 g $^{-1}$L PVP is the most suitable for use in DSSCs as they have the smallest particle sizes (20–40 nm) and porous characteristics. Typically, DSSCs using the ZnO film with an 8 μm-thickness can attain a comparatively high conversion efficiency of 4.57%. In order to further improve the energy conversion efficiency of DSSCs, a layer of compact nanocrystalline ZnO was pre-prepared by ECD in an electrolyte containing 0.01 M $Zn(NO_3)_2$ and 0.1 M KNO_3 solution without PVP, at a bath temperature of 0 °C under a potentiostatic condition of −1.3 V *vs.* SCE for 10 min. Subsequently, the 8 μm-thick nanoparticulate ZnO film was electrodeposited onto this nanocrystalline layer. The cell constructed with these double-layer ZnO nanocrystalline films prepared *via* two-step ECD yielded an impressive conversion efficiency of 5.08%. It was deduced that the improvement in cell performance could result from the fact that the presence of compact layer of ZnO can effectively suppress short circuiting and loss of current from recombination at the conducting glass electrode. This outstanding work proves that the ECD of double-layer nanocrystalline particulate ZnO films is a promising route to achieve cost-effective DSSCs.

Further, a one-step electrochemical codeposition route in the presence of certain organic molecules was developed by T. Yoshida to obtain highly porous ZnO nanoparticulate films.[180] In a typical coelectrodeposition,[181] upon cathodizing a conducting substrate in an O_2 saturated aqueous mixed solution of $ZnCl_2$ and eosin Y, ZnO/eosin Y nanoparticulate hybrid films with high crystallinity and high transparency were deposited (Fig. 22(b)). If eosin Y was not introduced, only pure hexagonal particles were formed (Fig. 22(a)). Note that the ECD of ZnO in the O_2 reduction system was controlled by both the charge transfer kinetics, that were varied with the electrode potential, and the mass transport that varies with the thickness of diffusion layer. Therefore, a rotating electrode system was adopted for homogeneous forced convection, so that a homogeneous thickness of the diffusion layer is achieved to obtain uniform thin films with high reproducibility. The hybrid ZnO/eosin Y films were characterized by high electron collection efficiency, and better electron transport properties[182] in the electrodeposited films than their colloidal counterparts, showing promising characteristics for use in DSSCs. A conversion efficiency of 0.8% can be obtained for a 1.4 μm-thick film under 20 mW cm^{-2} white light illumination.[183] Unlike the method used by T. Yoshida, X. Y. Gan *et al.*[184] adopted two-step ECD to prepare ZnO/eosin Y films. Here, a cathodic potential less than that commonly required for the deposition of ZnO was applied for 15 s to facilitate nucleation of ZnO nanocrystals on the substrate. It is found that this process can help to increase the crystallinity of resulting ZnO films and to enhance adherence

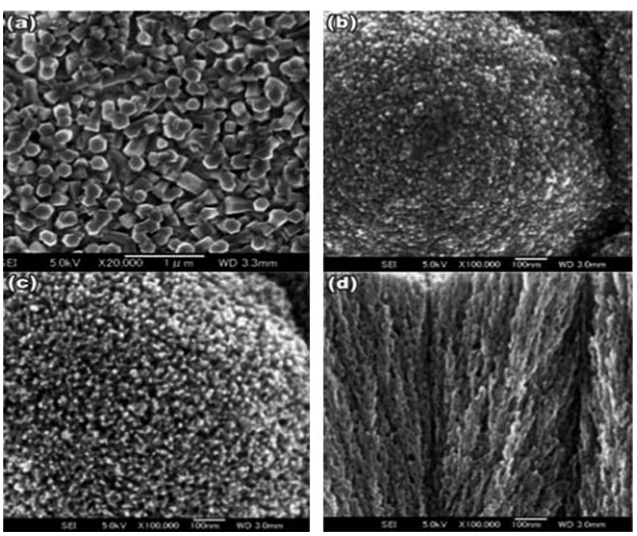

Fig. 22 SEM images of electrodeposited films: (a) Pure ZnO film deposited without eosin Y; (b) ZnO/eosin Y hybrid film; (c) porous nanoparticulate ZnO film obtained after extraction of eosin Y by soaking the ZnO/eosin Y hybrid film in diluted KOH aqueous solution, and (d) a cross-section view of the ZnO film corresponding to (c).[181,182]

between the film and the substrate. After the short pretreatment process, a series of ZnO/eosin Y films were grown potentiostatically with cathodic potentials from −0.8 V down to −1.1 V. The DSSC based on the prepared hybrid film with a thickness of 0.45 μm gave a conversion efficiency of 0.21%, open-circuit photovoltage of 0.64 V, and short-circuit photocurrent density of 0.67 mA cm^{-2}.[184]

As for the adsorption of eosin Y on the ZnO surface, a theoretical investigation was presented by F. Labat *et al.*[185] The results obtained highlight that eosin Y strongly adsorbs on the ZnO surface, contributing significantly to the electronic structure of the adsorbed system, and reveal that both the HOMO and the LUMO of eosin Y lie within the ZnO band gap and are exclusively localized on the dye. Thus, direct HOMO → LUMO excitation does not lead to electron injection into the semiconductor. As a consequence, a two photon injection mechanism is proposed to rationalize the low efficiency of the eosin Y/ZnO solar cells. Various strategies have been proposed to enhance the cell efficiency. For instance, replacing eosin Y by other dyes, but still using the porous nanoparticulate ZnO films, is a just as effective route. By soaking the hybrid ZnO/eosin Y films in soft alkaline solution, eosin Y can be completely removed with a large amount of nanopores formed within the films, as shown in Fig. 22(c) and (d).[181,182] By re-loading various dyes onto the surface of these films, highly transparent ZnO nanoparticulate films with plentiful colors are easily obtained. Also, ZnO films loaded with various dye photosensitizers can be effectively applied to flexible and colorful DSSCs. Owing to the superior properties of the films obtained under optimized conditions, the conversion efficiency of the DSSC employing D149 dye can reach 5.6% under illumination of AM1.5 simulated sun light (100 mW cm^{-2}).[181] The electrochemical codeposition with the eosin Y dye not only affected the morphology of nanoparticulate films, but also resulted in structural changes of electrodeposited ZnO matrices. H. Graaf *et al.*[186] demonstrated that during the desorption of eosin Y from ZnO films with aqueous KOH, the partial dissolving and reorganization of ZnO films took place. It is found that the reorganization led to a reduction of the oxygen defect concentration on the surface of ZnO nanoparticles, which is supposed to be a reason for suppressed recombination of electrons within the photoanodes of DSSCs.

The electrodeposition technique is also frequently utilized to prepare 1D ZnO nanostructured photoanodes. Well-aligned arrays of vertically oriented ZnO nanowires can be grown directly on ITO-coated glass and integrated into DSSCs, as shown in Fig. 23(a). T. Pauporte *et al.*[187] further studied the effect of annealing electrodeposited ZnO nanowires on the cell performance and demonstrated that the improvement in the conversion efficiency was ascribable to the elimination of intrinsic and extrinsic defects in as-electrodeposited ZnO nanowires. However, due to the adverse growth kinetics between the substrate and the crystal,[188] ultralong 1D nanostructure arrays with higher surface areas were seldom achieved by electrodeposition. From another point of view, increasing the surface roughness degree of electrodeposited 1D ZnO nanostructures can also increase their surface areas to some extent, which is slightly favorable for adsorbing more dye photosensitizers. Therefore, large-scale arrays of novel rhombus-shaped

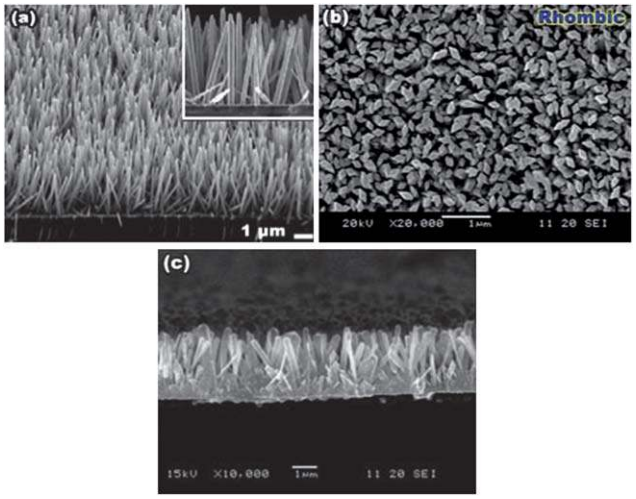

Fig. 23 SEM images of (a) ZnO nanowire arrays,[187] (b) top-view and (c) cross-section of rhombic ZnO nanorod arrays.[190]

polycrystalline ZnO nanorods with high surface roughness and mesoporous structures have been prepared by our group[189] and utilized as photoanodes to assemble DSSCs.[190] The rhombus-shaped ZnO nanorod arrays were made *via* a facile two-step synthesis strategy that involved firstly the electrodeposition of vertically aligned rhombic ZnF(OH) nanorod arrays from an aqueous electrolyte containing fluoride, and secondly the pyrolysis of a ZnF(OH) intermediate into ZnO with the same morphology. Typically, the electrodeposition of the rhombus-like ZnF(OH) nanorod arrays was potentiostatically performed at −1.1 V in an aqueous electrolyte containing 0.05 M $Zn(NO_3)_2$ and 0.1 M NaF using a classic three-electrode configuration that has been well documented. Subsequently, the as-obtained ZnF(OH) sample was pyrolyzed at 450 °C for 2 h to yield unique rhombus-like ZnO nanorod arrays, as shown in Fig. 23(b) and (c).[190] Note that since the rhombic ZnO nanorod arrays are derived from the ZnF(OH) nanorod arrays, the size of the ZnO nanorods are directly determined by that of the electrodeposited ZnF(OH) nanorods, which can be readily controlled by tuning the electrochemical parameters such as the electrolyte concentration and temperature, electrodeposition potential and duration, and the substrates. DSSCs based on the rhombus-like ZnO nanorod arrays with a larger roughness factor than the hexagon-like single-crystalline ZnO nanorod arrays, electrodeposited in the absence of NaF, exhibit higher conversion efficiency. By comparison, assuming nearly identical sizes, the better photovoltaic performance of rhombus-like ZnO nanorod arrays based DSSC should profit from better dye loading and light harvesting as a result of the enlargement of the internal surface area within the photoanode, which results from the rough surface characteristic of rhombus-like ZnO nanorods constructed by nanoparticles and nanopores. Although nanopores existed among the nanoparticles, they were tightly connected and not separated, which ensures good electrical conduction among adjacent nanoparticles.

In addition to 1D ZnO nanowire arrays, 2D ZnO sheet-like or belt-like arrays can also be prepared by ECD with the help of capping agents. A classic paradigm is that of L. F. Xu *et al.*[191,192] and our group,[193] who skilfully used the preferential adsorption

of Cl^- onto the (0001) planes of ZnO crystals to hinder crystal growth along the *c*-axis, resulting in the formation of ZnO nanosheet arrays. Fig. 24(a) presents a typical sheet-like morphology of ZnO nanosheets electrodeposited on ITO substrates at −1.1 V and 70 °C from 0.05 M $Zn(NO_3)_2$ and 0.06 M KCl solution.[192] Most of the nanosheets were vertical with respect to the substrate. By further ECD epitaxial growth of oriented nanorods on the surfaces of the ZnO nanosheets obtained by the first ECD, hierarchical ZnO nanorods on nanosheets were prepared (Fig. 24(b)).[192] When both the ZnO nanosheet arrays and the hierarchaical nanostructures were sensitized by N719 dye to act as photoanodes of DSSCs, conversion efficiencies of 0.48% and 0.74% were attained, respectively. Apparently, the latter higher conversion efficiency profited from a larger surface area within the hierarchical nanostructured photoanode, which resulted in an increase in the amount of dye absorbed and the corresponding conversion efficiency.

Electrodeposited ZnO nanosheets can not only be directly used as the photoanode, but can also be used to modify TiO_2-based DSSCs as the scattering layer, as shown in Fig. 25.[194] In this case, the FTO substrate coated with a sintered TiO_2 film was used as the working electrode, and an aqueous solution containing 0.25 M $ZnCl_2$ and 0.1 M KCl was used as the electrolyte. It was demonstrated that ZnO nanosheet modified TiO_2 nanoparticle-based DSSCs exhibited a higher conversion efficiency of 2.58% than the 1.79% for unmodified TiO_2 nanoparticle-based DSSCs, which could be attributed to the relatively high light harvesting efficiency of the former coming from effective light scattering.

As for the electrodeposited ZnO nanosheet arrays used in DSSCs, the difference in the dye sensitization process results in a difference in cell performance. However, fabricating a cell device to evaluate its performance is a tedious and laborious process. Thus, there is a need to develop a simple method which could be correlated with the performance to give a rough pre-evaluation of the actual cell performance after ECD of the ZnO nanosheet arrays. It is well known that surface wettability—which involves

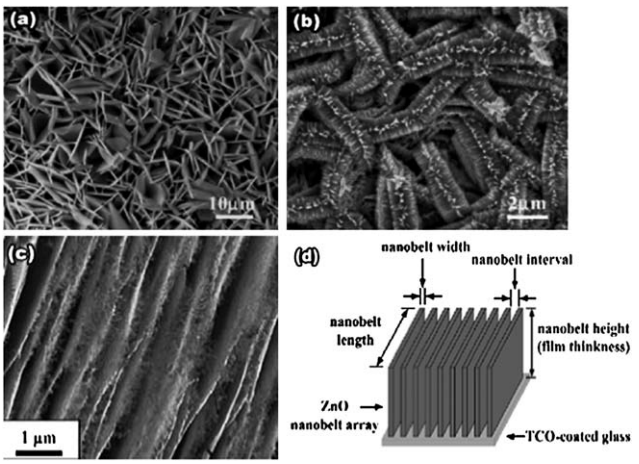

Fig. 24 SEM images of (a) ZnO nanosheet arrays and (b) hierarchical ZnO nanorods on nanosheets.[192] (c) SEM image and (d) schematic diagram of ZnO nanobelt array photoanode.[196]

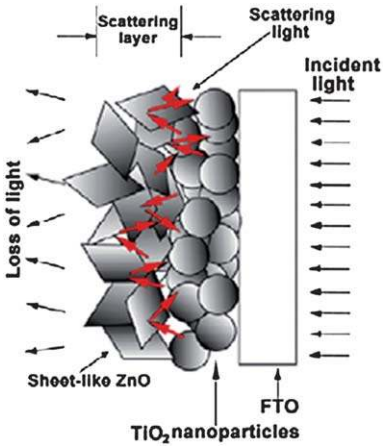

Fig. 25 Schematic diagram of light capture in ZnO nanosheets as the scattering layer in the TiO_2 nanoparticulate photoanode.[194]

the interaction between a liquid and a solid in contact—is an important parameter in surface science, and its measurement provides a simple and reliable technique for the interpretation of surface engineering. With this motivation, S. B. Ambade *et al.*[195] have developed a simple and economical approach by establishing an empirical diagnostic relationship between contact angle measurement (surface wettability) and solar-to-electrical conversion efficiency for electrodeposited ZnO nanosheet/N3 dye-based DSSCs. It is expected that this observed correlative trend is of scientific interest and might also be applicable to electrodes with different ZnO morphologies, and combinations of different dye-sensitizer molecules.

Another unique quasi 2D nanostructure, the ZnO nanobelt array, has also been successfully fabricated using an ECD method with a liquid crystal template.[196] The ECD was performed at 65 °C and −0.9 V *vs.* SCE for 5 h from an electrolytic solution containing 0.1 M $Zn(NO_3)_2$ and polyoxyethylene cetylether, which acts as a surfactant. After ECD, the as-prepared nanobelt arrays were amorphous and could be transformed into crystalline ZnO nanobelt arrays (Fig. 24(c)) after being sintered at 500 °C. Although the ZnO nanobelt array film is only 5 μm thick, the DSSC using this kind of ZnO nanobelt array photoanode (Fig. 24(d)) exhibited a high short-circuit photocurrent density of 17 mA cm^{-2}, and an overall power conversion efficiency of 2.6%.

4. Combined utilization of multiple solution methods

4.1. ACG/CBD for composite ZnO nanowire–nanoparticle photoanode

Various solution-processed ZnO nanostructures for use as photoanodes of DSSCs have been expatiated in the foregoing text and aim mainly at improving cell performance by either increasing the internal surface area within the photoanodes or providing rapid direct pathways for electron transport to the collecting electrodes. It is demonstrated that ZnO nanoparticulate film photoanodes characterized by a large internal surface area can adsorb more dye molecules for the capture of incident photons, but the electron recombination is relatively serious due to electron transport in the form of a series of hopping events between trap states on neighboring nanoparticles. The huge surface area also increases the

recombination between electrons in the conduction band of ZnO and the electron acceptor in the electrolyte. While the photoanodes with 1D or 2D ZnO nanostructure arrays, which have characteristic direct pathways for electron transport, can effectively reduce the recombination resulting from particle-boundary electron hopping or scattering, the cell conversion efficiency is limited to a low level. This is because of the low internal surface area intrinsically associated with the array structure. Therefore, with the intention of providing both the direct pathways for electron transport and large internal surface area for adsorbing more dye photosensitizers, ZnO photoanodes with hierarchical or composite nanostructures were developed one after the other by combined utilization of multiple solution methods. For instance, the incorporation of ZnO nanoparticles into ZnO nanowire arrays is a case in point. Typically, ZnO nanowire–nanoparticle films have been synthesized by Ku *et al.*[197] using an ACG–CBD method, and the synthesis route is described as follows: Firstly, the synthesis of ZnO nanowire arrays was performed by a seedlayer-induced ACG method, as explained in Section 3.2. Then, as-obtained ZnO nanowire arrays were immersed in a 0.15 M methanolic solution of $Zn(CH_3COO)_2$ at 60 °C for the CBD process of nanoparticles within the nanowire arrays. Fig. 26(a)–(d)[197] compares the morphology changes before and after CBD growth of the ZnO nanowire arrays for 18 h, showing that the intervals among ZnO nanowires have been densely filled with ZnO nanoparticles, but the film thickness is almost unchanged. It is demonstrated that using the 6.2 μm-thick ZnO nanowire–nanoparticle composite film sensitized by mercurochrome to construct the DSSC yielded a high conversion efficiency of 3.2%. According to the authors' explanation, the superior performance of the ZnO nanowire–nanoparticle composite DSSC is mainly ascribable to enrichment of the light harvesting without significantly sacrificing the electron transport efficiency. The introduction of ZnO nanoparticles into the ZnO nanowire arrays provides a larger internal surface area for dye adsorption. This results in increased light-harvesting, and single-crystalline ZnO nanowire arrays that provide direct pathways for rapid electron transport to the collecting conductive substrate still function, as shown in Fig. 26(e).[197] Whereafter, S. Yodyingyong *et al.*[198] also adopted thicker (11 μm) ZnO nanowire–nanoparticle films to obtain a higher conversion efficiency of 4.2%.

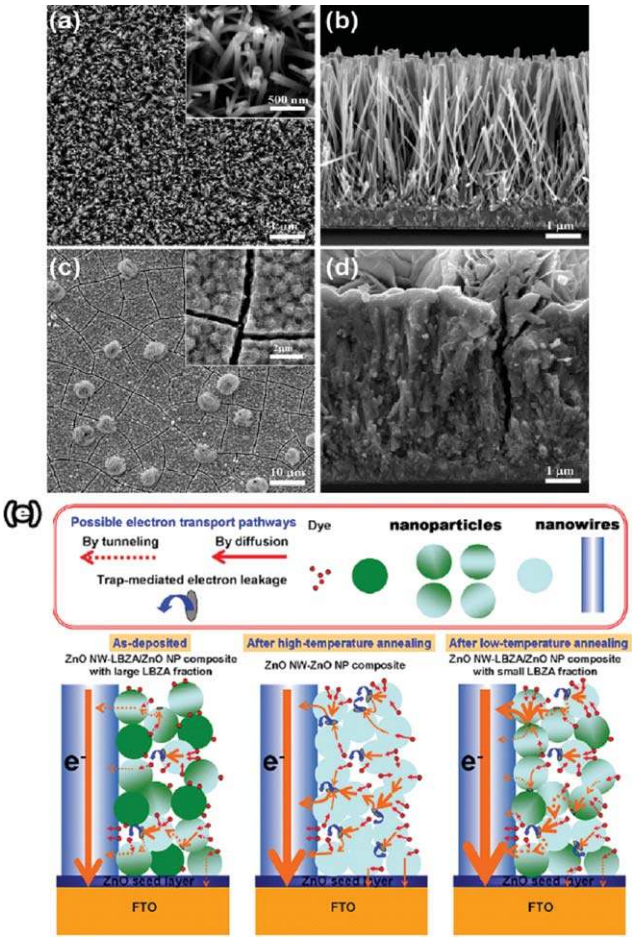

Fig. 26 (a) Top-view and (b) cross-section SEM images of ZnO nanowire arrays, and (c) a top-view and (d) cross-section SEM images of ZnO nanowire–nanoparticle composite structures after CBD of ZnO nanowire arrays for 18 h. (e) The possible electron transport mechanism within the photoanodes of ZnO nanowire–nanoparticle composite structures.[197]

4.2. ACG/Sol–Gel/ACG for branched ZnO nanowire photoanodes

ZnO nanowire–nanoparticle composite DSSCs with superior cell performances are developed with a consideration of increasing the amount of dye loading and retaining the rapid direct pathways resulting from nanowire arrays for electron transport. However, the excess electron hopping or scattering through the interparticle barriers might still increase the chance of carrier recombination. In this regard, nanostructures of tiny hierarchical nanobuilding units built into larger ordered conformations are intensely desirable from both the structural design and proposed application points of view. On the basis of the chemical vapor deposition (CVD), D. L. Suh *et al.*[199] and J. B. Baxter[127,128] have presented dendritic ZnO nanowires with efficiencies of about 0.5%. The relatively low energy conversion efficiencies for these early reports were due to insufficient surface area of the branched ZnO nanowires. Inspired by those early works, Cheng *et al.*[200] fabricated the treelike branched ZnO nanowire structures *via* the use of ACG/sol–gel/ACG methods. They firstly synthesized the arrays of ZnO nanowires on seeded FTO substrates by immersing the seeded substrates in aqueous solutions containing 0.08 M $Zn(NO_3)_2$, 0.08 M HMT, and 0.012 M PEI at 95 °C for 10 h, which is an ACG method. Secondly, the ZnO nanowire substrates obtained from the first step were recoated with seed layers of ZnO nanocrystallites by dip-coating in an ethanol solution of 0.005 M $Zn(CH_3COO)_2$, which belongs to a sol–gel process. Then the branched nanowires were re-grown *via* an ACG process by immersing the seeded ZnO nanowires in aqueous solutions containing 0.02 M $Zn(NO_3)_2$, 0.02 M HMT, and 0.003 M PEI, at 95 °C. The formation mechanism of the branched ZnO nanowires is illustrated in Fig. 27(a), and its corresponding SEM images in Fig. 27(b)–(d). Apparently, the branched ZnO nanowire structures with 1D secondary branches directly attached to the main ZnO nanowire backbone could simultaneously afford a direct conduction pathway and achieve the high dye adsorption, increasing significantly the overall conversion efficiency of the DSSC to 1.51%.

4.3. ECD-ACG for hierarchical ZnO nanosheet–nanowire photoanode

Although E. Hosono *et al.*[170–173] pioneered the fabrication of an upright-standing ZnO nanosheet array for use as the photoanode of DSSCs by CBD method, and attained a high conversion efficiency of 4.27%,[171] further improvement in cell performance is still desirable. Considering that branched architectures can readily grow on the surface of pre-prepared 1D ZnO nanostructure arrays by either the ACG method or the ECD technique, it is expected that in a similar manner, branched architectures can also be formed on the surface of 2D ZnO nanosheets by solution-phase synthesis methods. Recently, our group[201] has presented a two-step synthesis process based on the ECD-ACG methods to produce hierarchical ZnO nanosheet–nanowire architectures. Firstly, the arrays of hexagonal $Zn_5(OH)_8Cl_2$ nanosheets were electrodeposited on ITO substrates in the aqueous electrolyte of 0.05 M $Zn(NO_3)_2$ and 0.1 M KCl with a three-electrode electrochemical configuration, which can be found elsewhere.[176,177,202] The ECD was performed at −1.1 V and 50 °C for 30 min. Then, by thermal treatment at 350 °C or above in air, the obtained $Zn_5(OH)_8Cl_2$ nanosheets can be converted into ZnO nanosheets *via* solid-state crystal phase transformation, without altering the hexagonal sheet-like shape. Secondly, the hierarchical ZnO nanoarchitectures were grown *via* an ACG method by immersing the ZnO nanosheet substrate, obtained from the first step, into a bottle filled with an equimolar concentration (0.005 M) aqueous solution of $Zn(NO_3)_2$ and HMT, and kept at a constant temperature of 90 °C. The hierarchical ZnO nanoarchitectures rooted in ZnO nanosheet arrays were finally obtained. The evolution process of the hierarchical ZnO nanoarchitectures derived from ZnO nanosheet arrays is schematically illustrated in Fig. 28(a) and its corresponding SEM images are shown in Fig. 28(b)–(d). The DSSCs based on the hierarchical ZnO nanowire–nanosheet architectures showed a power conversion efficiency of 4.8%, which is nearly twice as high as that of the DSSC constructed using a photoanode of bare ZnO nanosheet arrays. The improved photovoltaic performance of the hierarchical ZnO nanoarchitecture DSSC was due to an improved dye loading and light harvesting capacity as a consequence of the enlargement of the internal surface area within the photoanode. Furthermore, the hierarchical ZnO nanowire–nanosheet architectures still retain the highly efficient direct pathways for electron transport, as shown in Fig. 28(e). It can be seen from Fig. 28(e) that the random wire-like branches attached to the main nanosheets are advantageous for a larger internal surface area and increased light–dye interactions, but without sacrificing the good electron transport, similar to upstanding nanosheet arrays, and ensuring the low recombination rate between the injected electrons and oxidized dye due to relatively rapid collection of photogenerated electrons. Although the gaps between the upright ZnO nanosheets have been filled with densely and randomly distributed ZnO nanowires, large numbers of interstices still exist (see Fig. 28(c)) and can provide enough space to transport the redox couple (I^-/I_3^-) between the electrodes. Likewise, this can also reduce the recombination rate between the injected electrons and tri-iodine ions in the electrolyte. In addition, the hierarchical ZnO nanowire–nanosheet architectures with dye loading can make the most of the photons falling in the gaps between adjacent ZnO nanosheets, avoiding incident light loss.

4.4. Sol–gel/HT for double-layer structured photoanode

Furthermore, a novel double light-scattering-layer ZnO (DL–ZnO) film, consisting of ZnO monodisperse aggregates (MA–ZnO) as an underlayer (Fig. 29(a)) and sub-micrometer-sized platelike ZnO (SP–ZnO) as an overlayer (Fig. 29(b)), was fabricated and studied for use as a DSSC photoanode.[203] SP–ZnO was synthesized by a hydrothermal process. Briefly, 0.1 M $Zn(CH_3COO)_2$ was mixed with 0.2 M NaOH and then transferred to Teflon-lined stainless steel autoclave kept at 180 °C for 10 h. The synthesis of MA–ZnO was extremely similar to the method developed by Zhang and Chou *et al.*[95–97] that has been widely adopted by succeeding researchers. Subsequently, the composite DL–ZnO film with bilayer structure (Fig. 29(c) and (d)) was constructed by sequentially drop-coating MA–ZnO as an underlayer photoanode and SP–ZnO particles as an

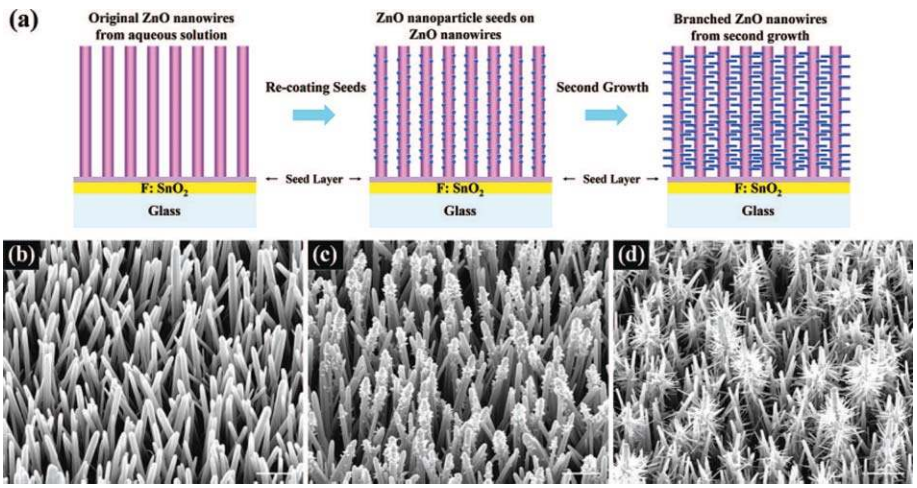

Fig. 27 (a) The schematic growth procedure from the original ZnO nanowires to the branched ZnO nanowires, (b) before and (c) after recoating a seed layer of the original ZnO nanowires obtained from a solvothermal method, and (d) the branched ZnO nanowires after second growth.[200]

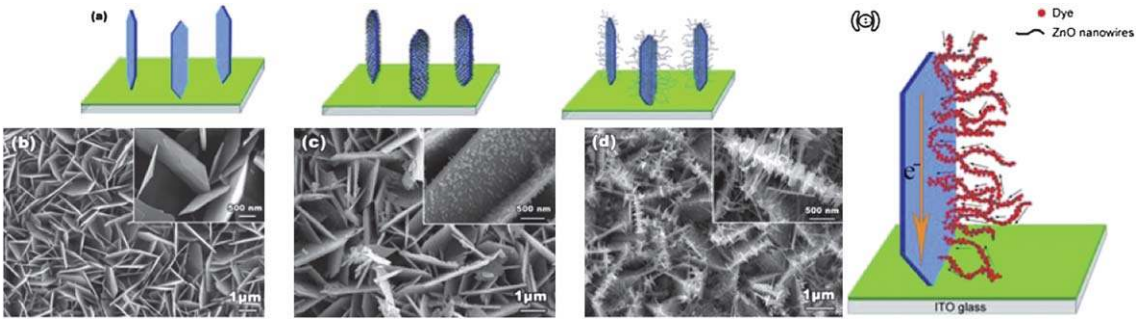

Fig. 28 (a) The schematic evolution process of the hierarchical ZnO nanoarchitectures derived from ZnO nanosheet arrays, and (b)–(d) top-view SEM images of the hierarchical ZnO nanowire–nanosheet architectures obtained by aqueous chemical growth after 0 h, 1 h and 4 h, respectively. The insets in (b)–(d) correspond to their magnified images. (e) Schematic diagram of the possible electron transport mechanism in hierarchical ZnO nanowire–nanosheet architecture photoanode of the DSSC.[201]

overlayer photoanode on an FTO substrate, followed by indispensable heating at 350 °C. It was found that DL–ZnO could significantly improve the conversion efficiency of DSSCs owing to its relatively high surface area and enhanced light-scattering capability. The overall power conversion efficiency of 3.44% was achieved by the formation of DL–ZnO film, which is 47% higher than that formed by MA–ZnO alone and far larger than that formed by SP–ZnO alone (0.81%).

5. Conclusions and outlook

Liquid-phase synthesis methods based on aqueous and nonaqueous solution systems of ZnO nanostructures for use as photoanodes in DSSCs have been reviewed in this article. The solution-derived ZnO nanostructured photoanodes include nanoparticulate films, 1D or 2D arrays, and hierarchical or composite nanostructures. Table 2 summarizes the majority of recent reports on DSSCs based on various ZnO nanostructures prepared by different solution synthesis methods. Among these solution synthesis methods, the sol–gel-derived nanoparticles and nanocrystallite aggregate films feature a large internal surface area that can load more dye photosensitizers or exhibit an efficient light-scattering effect, which results in more efficient light-harvesting. However, as the sol–gel method is generally based on nonaqueous solution systems, it may not be an environmentally sound technology due to the utilization of organic solvents. To reduce environmental damage and production cost, the HT synthesis method based on an aqueous solution system was developed to prepare ZnO nanoparticles as well as other nanostructures. In most cases, the hydrothermally synthesized ZnO products exist in the form of powder, and additional film-fabrication techniques such as the doctor-blade method or the screen-printing method are often needed to construct the photoanodes of DSSCs. Also, the unordered nanostructured photoanodes could encounter excess electron hopping or scattering during the electron transport through the nanostructure units, increasing the probability of electron recombination between the injected electrons and oxidized dye or redox couple in the electrolyte, and thus limiting an enhancement in the cell conversion efficiency. Therefore, the direct construction of photoanode films with 1D and 2D ZnO nanostructured arrays achieved by the ACG, CBD and ECD methods is desirable. As for 1D and 2D ZnO nanostructured arrays, the electrons directly transfer from the location where they inject to the collection electrode, with less electron scattering. This is different from the case of nanoparticulate films where the electrons take a random walk among the nanoparticles and encounter a large amount of scattering and collisions. Although the ACG and CBD methods can produce ordered 1D or 2D ZnO nanostructure array films on a large scale with a relatively low production cost, and as-prepared films can be directly integrated into DSSCs, the cell conversion efficiency is limited to a low level owing to the low internal surface area intrinsically associated with the array structure. Therefore, the ZnO photoanodes with hierarchical or composite nanostructures were developed by combined utilization of multiple solution methods. The hierarchical or composite nanostructures based on low-dimensional nanostructures are elegant because they could simultaneously provide large internal surface areas for dye loading, direct pathways for rapid electron transfer and collecting, or more light-scattering effects within the photoanodes for highly efficient incident photon capturing. With these improvements, deleterious electron recombination loss has

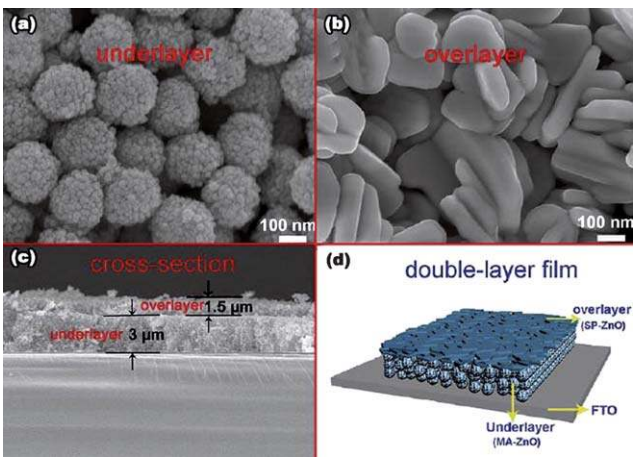

Fig. 29 SEM images of (a) monodisperse ZnO aggregates as an underlayer photoanode and (b) sub-micrometer-sized platelike ZnO particles as an overlayer photoanode, (c) cross-section SEM image of a double light-scattering-layer ZnO photoanode film, and (d) scheme of ZnO film based on double light-scattering-layer structure.[203]

Table 2 Summary of DSSCs based on solution-derived ZnO nanostructures

Synthesis method	Film preparation	Substrate	Photoanode structure (film thickness)	Dye	Light intensity/mW cm^{-2}	η (%)	Ref.
Sol–Gel	Dip-coating	FTO/glass	Nanoparticles (2–2.1 μm)	N3	100	0.8	79
	Doctor-blade	ITO/glass	Nanoparticles (Unknown)	Eosin-Y	100	0.45–1.11	80
	Spin-coating	FTO/glass	Nanoparticles (2 μm)	N3	100	0.92–2.5	81,82
	Compression	FTO/plastic	Nanoparticles (4–5 μm)	N719	10	1.4–5.0	73,74
	Drop-casting	FTO/glass	Nanocrystallite aggregates (9–10 μm)	N3	100	3.51–5.4	95 –97
HT	Doctor-blade	Unknown	Nanoparticles or nanosheets (6 μm)	N3	Unknown	0.75, 1.55	106
	Doctor-blade	FTO/glass	Nanosheet-spheres (12 μm)	N719	100	2.6	114
	Doctor-blade	FTO/glass	Nanoflowers (unknown)	N719	Unknown	1.37	115
	Doctor-blade	FTO/glass	Porous nanosheet assembly (12 μm)	N719	100	5.05	116
	Doctor-blade	ITO/glass	Nanoflowers modified with Au (unknown)	N3	100	2.5	117
	Spin-coating	FTO/glass	Nanoparticles doped with Sn (12 μm)	N719	100	3.79	118
	N/A	FTO/glass	Porous nanosheet array (unknown)	N719	Unknown	3.7	119
	Spray	FTO/glass	Nanoparticles (4.5 μm)	N3	Unknown	4.7	107
ACG	N/A	ZnO/FTO/glass	Nanowire array (8 μm)	N719	100	0.3	133
	N/A	ZnO/FTO/glass	Nanowire array (20–25 μm)	N719	100	1.2–1.5	35
	N/A	ZnO/ITO/glass	Nanowire array (33 μm)	N719	100	2.1	134
	N/A	ZnO/FTO/glass	Nanowire array (40 μm)	N719	100	1.3	139
	N/A	TiO_2/FTO/glass	Nanowire array (4 μm)	N719	100	2.15	140
	N/A	ZnO/FTO/glass	Nanowire array with TiO_2 shell (unknown)	N719	100	2.25	152
	N/A	ZnO/ITO/glass	Nanotube array (1 μm)	N3	Unknown	2.3	160
	N/A	Zn foil	Nanotips (3 μm)	N719	100	1.4	162
	N/A	FTO/glass	Nanoflower array (11 μm)	N719	100	1.9	165
CBD	N/A	FTO/glass	Nanosheet aggregates (65 μm)	Eosin-Y	10 or 100	3.31 or 2.0	174
	N/A	FTO/glass	Nanosheet array (4 μm)	N719	100	3.3	172
	N/A	FTO/glass	Nanosheet array (10 μm)	N719	100	3.9	170
	N/A	ITO/glass	Nanosheet array (20 μm)	N719	100	4.1	173
	N/A	FTO/glass	Nanosheet array (20 μm)	D149	100	4.27	171
ECD	N/A	ITO/glass	Nanoparticles (3.4 μm)	N719	100	1.02	178
	N/A	ZnO/FTO/glass	Nanoparticle film (8 μm)	N3	53	5.08	179
	N/A	FTO/glass	Nanoparticle/Eosin-Y film (1.4 μm)	Eosin-Y	20	0.8	183
	N/A	FTO/glass or plastic	Nanoparticles (unknown)	D149	100	5.6	181,182
	N/A	ITO/glass	Nanowire array (4.5 μm)	D149	100	0.66	187
	N/A	ITO/glass	Poly-crystalline nanorod array (3 μm)	D149	100	0.69	190
	N/A	ITO/glass	Nanosheet array (10 μm)	N719	100	0.48	192
	N/A	ITO/glass	Hierarchical nanorod/nanosheet (10 μm)	N719	100	0.74	192
	N/A	TiO_2/FTO/glass	Unordered nanosheets (2 μm)	N719	100	2.58	194
	N/A	ITO/glass	Nanobelt array (1.3 μm)	N719	100	2.6	196
ACG/Sol–Gel	N/A	ZnO/FTO/glass	Nanoparticles/nanowires (11 + 2 μm)	N3	Unknown	4.24	198
ACG/CBD	N/A	ZnO/FTO/glass	Nanoparticles/nanowires (5.5 μm)	Mercurochrome	100	3.2	197
ACG/Sol–Gel/ACG	N/A	ZnO/FTO/glass	Branched nanowires (7–8 μm)	N719	100	1.51	200
ECD/ACG	N/A	ITO/glass	Hierarchical nanosheets/nanowires (5 μm)	N719	100	4.8	201
Sol–Gel/HT	Drop-coating	FTO/glass	Double-layer nanocrystallite aggregates and microplates (3 + 1.5 μm)	N3	100	3.44	203

been effectively suppressed to some extent, and incident light can be absorbed more adequately, resulting in a sequential enhancement in ZnO-based DSSC performance.

In conclusion, the chemically based solution-phase methods mentioned above are inherently relatively facile and economical, readily scalable for mass production for fabrication of photoanodes for DSSCs, unlike the corresponding physical or chemical vapor-phase methods that need high energy and costly equipment to handle high vacuum and temperature. Furthermore, solution-phase methods can be fully competent for the task assumed by other synthesis methods only by the optimization of solution-phase system. Thus, the solution-phase synthesis methods of ZnO nanostructures reviewed are of great interest not only from the view point of basic science but also for practical applications. It is worthwhile to note that in the future, the combined use of multifold solution synthesis methods will be a potent measure to develop new hierarchical or composite ZnO nanostructures, and thus is expected to play a significant role in improving the photoanode configuration and enhancing the overall performance of the DSSCs.

Acknowledgements

This work was supported by the National Basic Research Program of China (973 Program, Grant Nos. 2011CB707601 and 2009CB623702), the National Natural Science Foundation of China (NNSFC, Grant Nos. 51071044 and 60976003), China Postdoctoral Science Foundation Funded Project (Grant No. 20100470066), Jiangsu Planned Projects for Postdoctoral Research Funds (Grant No. 0902003B), and Open Research Fund of State Key Laboratory of Bioelectronics.

References

1 *Basic Research Needs for Solar Energy Utilization*, U.S. Department of Energy, 2005.
2 S. Tarver, *Environ. Sci. Technol.*, 1974, **8**, 294.
3 A. Weisbrich, *Environ. Sci. Technol.*, 1979, **13**, 1445.
4 F. Tasca, L. Gorton, W. Harreither, D. Haltrich, R. Ludwig and G. Noll, *J. Phys. Chem. C*, 2008, **112**, 9956.
5 D. Fairless, *Nature*, 2007, **449**, 652.
6 W. E. Mabee, *Adv. Biochem. Eng./Biotechnol.*, 2007, **108**, 329.
7 V. Cermak and V. M. Hamza, *Int. J. Earth Sci.*, 2008, **97**, 201.
8 M. Hara, *Energy Environ. Sci.*, 2010, **3**, 601.
9 P. J. le, B. Williams and L. M. L. Laurens, *Energy Environ. Sci.*, 2010, **3**, 554.
10 W. Hooffmann, *Sol. Energy Mater. Sol. Cells*, 2006, **90**, 3285.
11 L. M. Goncalves, V. Z. Bermudez, H. A. Ribeiro and A. M. Mendes, *Energy Environ. Sci.*, 2008, **1**, 655.
12 D. Chapin, C. Fuller and G. Pearson, *J. Appl. Phys.*, 1954, **25**, 676.
13 K. L. Chopra, P. D. Paulson and V. Dutta, *Progr. Photovolt.: Res. Appl.*, 2004, **12**, 69.
14 R. B. Bergmann, *Appl. Phys. A: Mater. Sci. Process.*, 1999, **69**, 187.
15 A. Shah, P. Torres, R. Tscharner, N. Wyrsch and H. Keppner, *Science*, 1999, **285**, 692.
16 D. Carlson and C. Wronski, *Appl. Phys. Lett.*, 1976, **28**, 671.
17 D. Staebler and C. Wronski, *Appl. Phys. Lett.*, 1977, **31**, 292.
18 D. Cusano, *Solid-State Electron.*, 1963, **6**, 217.
19 M. Green, K. Emery, Y. Hishikawa and W. Warta, *Progr. Photovolt.: Res. Appl.*, 2008, **16**, 435.
20 A. Morales-Acevedo, *Sol. Energy Mater. Sol. Cells*, 2006, **90**, 2213.
21 D. Morgan, C. Shines, S. Jeter, M. Blazka, M. Elwell, R. Wilson, S. Ward, H. Price and P. Moskowitz, *Toxicol. Appl. Pharmacol.*, 1997, **147**, 399.
22 S. Cho, D. Maysinger, M. Jain, B. Roder, S. Hackbarth and F. Winnik, *Langmuir*, 2007, **23**, 1974.
23 L. Kazmerski, F. White and G. Morgan, *Appl. Phys. Lett.*, 1976, **29**, 268.
24 B. Dimmler and H. Schock, *Progr. Photovolt.: Res. Appl.*, 1996, **4**, 425.
25 R. W. Birkmire, *Sol. Energy Mater. Sol. Cells*, 2001, **65**, 17.
26 M. Bosi and C. Pelosi, *Progr. Photovolt.: Res. Appl.*, 2007, **15**, 51.
27 D. M. Li, D. Qin, M. H. Deng, Y. H. Luo and Q. B. Meng, *Energy Environ. Sci.*, 2009, **2**, 283.
28 T. W. Hamann, R. A. Jensen, A. B. F. Martinson, H. V. Ryswyk and J. T. Hupp, *Energy Environ. Sci.*, 2008, **1**, 66, permission to publish granted.
29 M. Gratzel, *Nature*, 2001, **414**, 338.
30 B. O'Regan and M. Gratzel, *Nature*, 1991, **353**, 737.
31 M. K. Nazeeruddin, F. D. Angelis, S. Fantacci, A. Selloni, G. Viscardi, P. Liska, S. Ito, B. Takeru and M. Gratzel, *J. Am. Chem. Soc.*, 2005, **127**, 16835.
32 J. Nissfolk, K. Fredin, A. Hagfeldt and G. Boschloo, *J. Phys. Chem. B*, 2006, **110**, 17715.
33 M. Gratzel, *Inorg. Chem.*, 2005, **44**, 6841.
34 M. Gratzel, *J. Photochem. Photobiol., A*, 2004, **164**, 3.
35 M. Law, L. E. Greene, J. C. Johnson, R. Saykally and P. D. Yang, *Nat. Mater.*, 2005, **4**, 455.
36 M. Saito and S. Fujihara, *Energy Environ. Sci.*, 2008, **1**, 280.
37 G. Shen, J. H. Cho and C. J. Lee, *Chem. Phys. Lett.*, 2005, **401**, 414.
38 A. Khan and M. Kordesch, *Phys. E.*, 2005, **30**, 51.
39 C. H. Ye, X. S. Fang, Y. F. Hao, X. M. Teng and L. D. Zhang, *J. Phys. Chem. B*, 2005, **109**, 19758.
40 W. H. Chiu, C. H. Lee, H. M. Cheng, H. F. Lin, S. C. Liao, J. M. Wu and W. F. Hsieh, *Energy Environ. Sci.*, 2009, **2**, 694.
41 S. Muthukumar, C. R. Gorla, N. W. Emanetoglu, S. Liang and Y. Lu, *J. Cryst. Growth*, 2001, **225**, 197.
42 Z. Z. Zhang, D. Z. Shen, Y. M. Lu, J. Y. Zhang, B. H. Li, D. X. Zhao, B. Yao and X. W. Fan, *J. Lumin.*, 2007, **122–123**, 202.
43 Z. B. Ayadi, L. E. Mir, K. Djessas and S. Alaya, *Mater. Sci. Eng., C*, 2008, **28**, 613.
44 I. Gonzalez-Valls and M. Lira-Cantu, *Energy Environ. Sci.*, 2010, **3**, 789.
45 Q. F. Zhang, C. S. Dandeneau, X. Y. Zhou and G. Z. Cao, *Adv. Mater.*, 2009, **21**, 4087.
46 I. Gonzalez-Valls and M. Lira-Cantu, *Energy Environ. Sci.*, 2009, **2**, 19.
47 R. Jose, V. Thavasi and S. amakrishna, *J. Am. Ceram. Soc.*, 2009, **92**, 289.
48 K. H. Yu and J. H. Chen, *Nanoscale Res. Lett.*, 2009, **4**, 1.
49 J. M. Kroon, N. J. Bakker, H. J. P. Smit, P. Liska, K. R. Thampi, P. Wang, S. M. Zakeeruddin, M. Gratzel, A. Hinsch, S. Hore, U. Wurfel, R. Sastrawan, J. R. Durrant, E. Palomares, H. Pettersson, T. Gruszecki, J. Walter, K. Skupien and G. E. Tulloch, *Progr. Photovolt.: Res. Appl.*, 2007, **15**, 1.
50 T. W. Hamann, R. A. Jensen, A. B. F. Martinson, H. V. Ryswyk and J. T. Hupp, *Energy Environ. Sci.*, 2008, **1**, 66.
51 M. Pagliaro, G. Palmisano, R. Ciriminna and V. Loddo, *Energy Environ. Sci.*, 2009, **2**, 838.
52 Y. H. Luo, D. M. Li and Q. B. Meng, *Adv. Mater.*, 2009, **21**, 4647.
53 D. M. Li, D. Qin, M. H. Deng, Y. H. Luo and Q. B. Meng, *Energy Environ. Sci.*, 2009, **2**, 283.
54 H. J. Snaith and L. Schmidt-Mende, *Adv. Mater.*, 2007, **19**, 3187.
55 V. Thavasi, V. Renugopalakrishnan, R. Jose and S. Ramakrishna, *Mater. Sci. Eng., R*, 2009, **63**, 81.
56 J. H. Yum, R. Humphry-Baker, S. M. Zakeeruddin, M. K. Nakeeruddin and M. Gratzel, *Nano Today*, 2010, **5**, 91.
57 Z. J. Ning, Y. Fu and H. Tian, *Energy Environ. Sci.*, 2010, **3**, 1170.
58 D. Wei, *Int. J. Mol. Sci.*, 2010, **11**, 1103.
59 S. M. Zakeeruddin and M. Gratzel, *Adv. Funct. Mater.*, 2009, **19**, 2187.
60 J. J. Lagref, M. K. Nakeeruddin and M. Gratzel, *Inorg. Chim. Acta*, 2008, **361**, 735.
61 M. Gratzel, *J. Photochem. Photobiol., C*, 2003, **4**, 145.
62 M. Gratzel, *J. Photochem. Photobiol., A*, 2004, **164**, 3.
63 G. Boschloo and A. Hagfeldt, *Acc. Chem. Res.*, 2009, **42**, 1819.
64 H. Gerischer and H. Tributsch, *Ber. Bunsen-Ges. Phys. Chem.*, 1968, **72**, 437.
65 H. Tributsch, *Photochem. Photobiol.*, 2008, **16**, 261.
66 L. Spanhel and M. A. Anderson, *J. Am. Chem. Soc.*, 1991, **113**, 2826.
67 K. Keis, L. Vayssieres, H. Rensmo, S. E. Lindquist and A. Hagfeldt, *J. Electrochem. Soc.*, 2001, **148**, A149.

68 S. Rani, P. Suri, P. K. Shishodia and R. M. Mehra, *Sol. Energy Mater. Sol. Cells*, 2008, **92**, 1639.
69 G. Redmond, D. Fitzmaurice and M. Graetzel, *Chem. Mater.*, 1994, **6**, 686.
70 A. I. Kontos, A. G. Kontos, D. S. Tsoukleris, M. C. Bernard, N. Spyrellis and P. Falaras, *J. Mater. Process. Technol.*, 2008, **196**, 243.
71 D. S. Zhang, S. Ito, Y. J. Wada, T. Kitamura and S. Yanagida, *Chem. Lett.*, 2001, 1042.
72 M. Wu, Z. H. Yang, Y. H. Jiang, J. J. Zhang, S. Q. Liu and Y. M. Sun, *J. Solid State Electrochem.*, 2010, **14**, 857.
73 K. Keis, C. Bauer, G. Boschloo, A. Hagfeldt, K. Westermark, H. Rensmo and H. Siegbahn, *J. Photochem. Photobiol., A*, 2002, **148**, 57, permission to publish granted.
74 K. Keis, E. Magnusson, H. Lindstrom, S. E. Lindquist and A. Hagfeldt, *Sol. Energy Mater. Sol. Cells*, 2002, **73**, 51.
75 H. Lindstrom, A. Holmberg, E. Magnusson, S. E. Lindquist, L. Malmqvist and A. Hagfeldt, *Nano Lett.*, 2001, **1**, 97.
76 L. Zhu, Y. Q. Fan, M. C. Zhao, M. Wu, J. Y. Zhang, C. X. Xu and Y. P. Cui, *Chin. Phys. Lett.*, 2009, **26**, 018401.
77 L. L. Lu, R. J. Li, K. Fan and T. Y. Peng, *Sol. Energy*, 2010, **84**, 844.
78 S. Ueno and S. Fujihara, *Eur. J. Inorg. Chem.*, 2010, 2165.
79 M. F. Hossain, S. Biswas, M. Shahjahan and T. Takahashi, *J. Vac. Sci. Technol., A*, 2009, **27**, 1047.
80 S. Rani, P. Suri, P. K. Shishodia and R. M. Mehra, *Sol. Energy Mater. Sol. Cells*, 2008, **92**, 1639.
81 M. C. Kao, H. Z. Chen, S. L. Young, C. Y. Kung, C. C. Lin and J. Z. Lai, *J. Supercond. Novel Magn.*, 2010, **23**, 897.
82 M. C. Kao, H. Z. Chen and S. L. Young, *Appl. Phys. A: Mater. Sci. Process.*, 2010, **98**, 595, permission to publish granted.
83 T. W. Hamann, A. B. F. Martinson, J. W. Elam, M. J. Pellin and J. T. Hupp, *Adv. Mater.*, 2008, **20**, 1560.
84 J. Ferber and J. Luther, *Sol. Energy Mater. Sol. Cells*, 1998, **54**, 265.
85 A. Usami, *Chem. Phys. Lett.*, 1997, **277**, 105.
86 G. Rothenberger, P. Comte and M. Gratzel, *Sol. Energy Mater. Sol. Cells*, 1999, **58**, 321.
87 S. Hore, P. Nitz, C. Vetter, C. Prahl, M. Niggemann and R. Kern, *Chem. Commun.*, 2005, 2011.
88 C. Anderson and A. J. Bard, *J. Phys. Chem. B*, 1997, **101**, 2611.
89 C. J. Barbe, F. Arendse, P. Comte, M. Jirousek, F. Lenzmann, V. Shklover and M. Gratzel, *J. Am. Ceram. Soc.*, 2005, **80**, 3157.
90 W. W. So, K. J. Kim, J. K. Lee and S. J. Moon, *Jpn. J. Appl. Phys.*, 2004, **43**, 1231.
91 C. Anderson and A. J. Bard, *J. Phys. Chem. B*, 1997, **101**, 2611.
92 C. J. Barbe, F. Arendse, P. Comte, M. Jirousek, F. Lenzmann, V. Shklover and M. Gratzel, *J. Am. Ceram. Soc.*, 2005, **80**, 3157.
93 S. Hore, P. Nitz, C. Vetter, C. Prahl, M. Niggemann and R. Kern, *Chem. Commun.*, 2005, 2011.
94 L. Yang, Y. Lin, J. G. Jia, X. R. Xiao, X. P. Li and X. W. Zhou, *J. Power Sources*, 2008, **182**, 370.
95 T. P. Chou, Q. F. Zhang, G. E. Fryxell and G. Z. Cao, *Adv. Mater.*, 2007, **19**, 2588.
96 Q. F. Zhang, T. R. Chou, B. Russo, S. A. Jenekhe and G. Z. Cao, *Angew. Chem., Int. Ed.*, 2008, **47**, 2402, permission to publish granted.
97 Q. F. Zhang, T. P. Chou, B. Russo, S. A. Jenekhe and G. Z. Cao, *Adv. Funct. Mater.*, 2008, **18**, 1654.
98 D. Jezequel, J. Guenot, N. Jouini and F. Fievet, *Mater. Sci. Forum*, 1994, **152–153**, 339.
99 E. W. Seelig, B. Tang, A. Yamilov, H. Cao and R. P. H. Chang, *Mater. Chem. Phys.*, 2003, **80**, 257.
100 H. M. Cheng, H. C. Hsu, S. L. Chen, W. T. Wu, C. C. Kao, L. J. Lin and W. F. Hsieh, *J. Cryst. Growth*, 2005, **277**, 192.
101 H. M. Cheng, K. F. Lin, H. C. Hsu, C. J. Lin, L. J. Lin and W. F. Hsieh, *J. Phys. Chem. B*, 2005, **109**, 18385.
102 H. M. Cheng and W. F. Hsieh, *Energy Environ. Sci.*, 2010, **3**, 442.
103 Y. Z. Zhang, L. H. Wu, Y. P. Liu and E. Q. Xie, *J. Phys. D: Appl. Phys.*, 2009, **42**, 085105, permission to publish granted.
104 Y. Z. Zhang, L. H. Wu, Y. P. Liu, E. Q. Xie, D. Yan and J. T. Chen, *Chin. Phys. Lett.*, 2009, **26**, 038201.
105 J. C. Tao, Y. Sun, M. Y. Ge, X. Chen and N. Dai, *J. Infrared Millimeter Waves*, 2010, **29**, 1.
106 A. E. Suliman, Y. W. Tang and L. Xu, *Sol. Energy Mater. Sol. Cells*, 2007, **91**, 1658, permission to publish granted.
107 A. Ranga Rao and V. Dutta, *Nanotechnology*, 2008, **19**, 445712.
108 A. Ranga Rao and V. Dutta, *Phys. Status Solidi A*, 2004, **201**, R72.
109 M. Y. Song, D. K. Kim, K. J. Ihn, S. M. Jo and D. Y. Kim, *Nanotechnology*, 2004, **15**, 1861.
110 R. Jose, A. Kumar, V. Thavasi and S. Ramakrishna, *Nanotechnology*, 2008, **19**, 424004.
111 X. G. Han, H. Z. He, Q. Kuang, X. Zhou, X. H. Zhang, T. Xu, Z. X. Xie and L. S. Zheng, *J. Phys. Chem. C*, 2009, **113**, 584.
112 H. Zhang, D. R. Yang, D. S. Li, X. Y. Ma, S. Z. Li and D. L. Que, *Cryst. Growth Des.*, 2005, **5**, 547.
113 H. M. Hu, X. H. Huang, C. H. Deng, X. Y. Chen and Y. T. Qian, *Mater. Chem. Phys.*, 2007, **106**, 58.
114 M. S. Akhtar, M. A. Khan, M. S. Jeon and O. B. Yang, *Electrochim. Acta*, 2008, **53**, 7869, permission to publish granted.
115 C. X. Wang, X. D. Zhang, D. F. Wang, Z. H. Yang, W. W. Ji, C. S. Zhang and Y. Zhao, *Sci. China, Ser. E: Technol. Sci.*, 2010, **53**, 1146, permission to publish granted.
116 Y. C. Qiu, W. Chen and S. H. Yang, *J. Mater. Chem.*, 2010, **20**, 1001, permission to publish granted.
117 V. Dhas, S. Muduli, W. Lee, S. H. Han and S. Ogale, *Appl. Phys. Lett.*, 2008, **93**, 243108, permission to publish granted.
118 N. Ye, J. J. Qi, Z. Qi, X. M. Zhang, Y. Yang, J. Liu and Y. Zhang, *J. Power Sources*, 2010, **195**, 5806.
119 X. Y. Wang, Z. P. Tian, T. Yu, H. M. Tian, J. Y. Zhang, S. K. Yuan, X. B. Zhang, Z. S. Li and Z. G. Zou, *Nanotechnology*, 2010, **21**, 065703, permission to publish granted.
120 O. Dulub, L. A. Boatner and U. Diebold, *Surf. Sci.*, 2002, **519**, 201.
121 B. Pradhan, S. K. Batabyal and A. J. Pal, *Sol. Energy Mater. Sol. Cells*, 2007, **91**, 769.
122 G. M. Hua, Y. Zhang, J. X. Zhang, X. L. Cao, W. Xu and L. D. Zhang, *Mater. Lett.*, 2008, **62**, 4109.
123 Y. J. Lee, D. S. Ruby, D. W. Peters, B. B. Mckenzie and J. W. P. Hsu, *Nano Lett.*, 2008, **8**, 1501.
124 M. Guo, P. Diao, X. D. Wang and S. M. Cai, *J. Solid State Chem.*, 2005, **178**, 3210.
125 Y. F. Gao and M. Nagai, *Langmuir*, 2006, **22**, 3936.
126 A. B. F. Martinson, J. E. McGarrah, M. O. K. Parpia and J. T. Hupp, *Phys. Chem. Chem. Phys.*, 2006, **8**, 4655.
127 J. B. Baxter and E. S. Aydil, *Sol. Energy Mater. Sol. Cells*, 2006, **90**, 607.
128 J. B. Baxter and E. S. Aydil, *Appl. Phys. Lett.*, 2005, **86**, 053114.
129 L. Vayssieres, K. Keis, A. Hagfeldt and S. E. Lindquist, *Chem. Mater.*, 2001, **13**, 4395.
130 L. Vayssieres, *Int. J. Nanotechnol.*, 2004, **1**, 1.
131 L. Vayssieres, *Adv. Mater.*, 2003, **15**, 464.
132 L. Vayssieres, A. Hagfeldt and S. E. Lindquist, *Pure Appl. Chem.*, 2000, **72**, 47.
133 J. B. Baxter, A. M. Walker, K. van Ommering and E. S. Aydil, *Nanotechnology*, 2006, **17**, S304, permission to publish granted.
134 C. K. Xu, P. Shin, L. L. Cao and D. Gao, *J. Phys. Chem. C*, 2010, **114**, 125, permission to publish granted.
135 Y. F. Hsu, Y. Y. Xi, A. B. Djurisic and W. K. Chan, *Appl. Phys. Lett.*, 2008, **92**, 133507.
136 L. E. Greene, M. Law, D. H. Tan, M. Montano, J. Goldberger, G. Somorjai and P. D. Yang, *Nano Lett.*, 2005, **5**, 1231.
137 R. S. Mane, W. J. Lee, C. D. Lokhande, B. W. Cho and S. H. Han, *Curr. Appl. Phys.*, 2008, **8**, 549.
138 H. M. Gao, G. J. Fang, M. J. Wang, N. S. Liu, L. Y. Yuan, C. Li, L. Ai, J. Zhang, C. H. Zhou, S. J. Wu and X. Z. Zhao, *Mater. Res. Bull.*, 2008, **43**, 3345.
139 J. J. Qiu, X. M. Li, F. W. Zhuge, X. Y. Gan, X. D. Gao, W. Z. He, S. J. Park, H. K. Kim and Y. H. Hwang, *Nanotechnology*, 2010, **21**, 195602.
140 Y. Q. Wang, Y. M. Sun and K. Li, *Mater. Lett.*, 2009, **63**, 1102, permission to publish granted.
141 M. H. Lai, A. Tubtimtae, M. W. Lee and G. J. Wang, *Int. J. Photoenergy*, 2010, 497095.
142 S. H. Lee, S. H. Han, H. S. Jung, H. Shin, J. Lee, J. H. Noh, S. Lee, I. S. Cho, J. K. Lee, J. Kim and H. Shin, *J. Phys. Chem. C*, 2010, **114**, 7185.
143 H. H. Chen, A. D. Pasquier, G. Saraf, J. Zhang and Y. C. Lu, *Semicond. Sci. Technol.*, 2008, **23**, 045004.
144 H. H. Chen, Z. Q. Duan, Y. C. Lu and A. D. Pasquier, *J. Electron. Mater.*, 2009, **38**, 1612.
145 A. D. Pasquier, H. H. Chen and Y. C. Lu, *Appl. Phys. Lett.*, 2006, **89**, 253513.
146 C. He, Z. Zeng, H. L. Tang, L. N. Zhao and F. Lu, *J. Phys. Chem. C*, 2009, **113**, 10322.

147 Y. Diamant, S. G. Chen, O. Melamed and A. Zaban, *J. Phys. Chem. B*, 2003, **107**, 1977.
148 A. Zaban, S. G. Chen, S. Chappel and B. A. Gregg, *Chem. Commun.*, 2000, 2231.
149 Y. J. Shin, J. H. Lee, J. H. Park and N. G. Park, *Chem. Lett.*, 2007, **36**, 1506.
150 K. M. P. Bandaranayake, M. K. I. Senevirathna, P. M. G. M. P. Weligamuwa and K. Tennakone, *Coord. Chem. Rev.*, 2004, **248**, 1277.
151 M. Law, L. E. Greene, A. Radenovic, T. Kuykendall, J. Liphardt and P. D. Yang, *J. Phys. Chem. B*, 2006, **110**, 22652.
152 Y. Diamant, S. Chappel, S. G. Chen, O. Melamed and A. Zaban, *Coord. Chem. Rev.*, 2004, **248**, 1271.
153 J. J. Wu, G. R. Chen, H. H. Yang, C. H. Ku and J. Y. Lai, *Appl. Phys. Lett.*, 2007, **90**, 213109.
154 G. W. She, X. H. Zhang, W. S. Shi, X. Fan, J. C. Chang, C. S. Lee, S. T. Lee and C. H. Liu, *Appl. Phys. Lett.*, 2008, **92**, 053111.
155 G. W. She, X. H. Zhang, W. S. Shi, X. Fan and J. C. Chang, *Electrochem. Commun.*, 2007, **9**, 2784.
156 C. L. Yan and D. F. Xue, *Electrochem. Commun.*, 2007, **9**, 1247.
157 L. F. Xu, Q. Liao, J. P. Zhang, X. C. Ai and D. S. Xu, *J. Phys. Chem. C*, 2007, **111**, 4549.
158 C. C. Wang, K. Yu, L. J. Li, Q. Li and Z. Q. Zhu, *Appl. Phys. A: Mater. Sci. Process.*, 2008, **90**, 739.
159 J. Elias, R. Tena-Zaera, G. Y. Wang and C. Levy-Clement, *Chem. Mater.*, 2008, **20**, 6633.
160 M. Guo, P. Diao and S. M. Cai, *Chin. Chem. Lett.*, 2004, **15**, 1113, permission to publish granted.
161 A. B. F. Martinson, J. W. Elam, J. T. Hupp and M. J. Pellin, *Nano Lett.*, 2007, **7**, 2183.
162 Z. Z. Yang, T. Xu, Y. Ito, U. Welp and W. K. Kwok, *J. Phys. Chem. C*, 2009, **113**, 20521, permission to publish granted.
163 C. Y. Kuan, J. M. Chou, I. C. Leu and M. H. Hon, *J. Mater. Res.*, 2008, **23**, 1163.
164 C. Y. Kuan, J. M. Chou, I. C. Leu and M. H. J. Hon, *Electrochem. Commun.*, 2007, **9**, 2093.
165 C. Y. Jiang, X. W. Sun, G. Q. Lo, D. L. Kwong and J. X. Wang, *Appl. Phys. Lett.*, 2007, **90**, 263501, permission to publish granted.
166 F. P. Yan, L. H. Huang, J. S. Zheng, J. Huang, Z. Lin, F. Huang and M. D. Wei, *Langmuir*, 2010, **26**, 7153.
167 C. D. Lokhande, P. M. Gondkar, R. S. Mane, V. R. Shinde and S. H. Han, *J. Alloys Compd.*, 2009, **475**, 304.
168 B. C. Bunker, P. C. Rieke, B. J. Tarasevich, A. A. Campbell, G. E. Fryxell, G. L. Graff, J. Liu, J. W. Virden and G. L. McVay, *Science*, 1994, **264**, 48.
169 E. Hosono, S. Fujihara, T. Kimura and H. Imai, *J. Colloid Interface Sci.*, 2004, **272**, 391.
170 E. Hosono, S. Fujihara, I. Honna and H. S. Zhou, *Adv. Mater.*, 2005, **17**, 2091.
171 E. Hosono, Y. Mitsui and H. S. Zhou, *Dalton Trans.*, 2008, 5439.
172 K. Kakiuchi, M. Saito and S. Fujihara, *Thin Solid Films*, 2008, **516**, 2026, permission topublish granted.
173 K. Kakiuchi, E. Hosono and S. Fujihara, *J. Photochem. Photobiol., A*, 2006, **179**, 81.
174 E. Hosono, S. Fujihara and T. Kimura, *Electrochim. Acta*, 2004, **49**, 2287, permission to publish granted.
175 R. Zhang, J. Pan, E. P. Briggs, M. Thrash and L. L. Kerr, *Sol. Energy Mater. Sol. Cells*, 2008, **92**, 425, permission to publish granted.
176 M. Izaki and T. Omi, *Appl. Phys. Lett.*, 1996, **68**, 2439.
177 S. Peulon and D. Lincot, *Adv. Mater.*, 1996, **8**, 166.
178 Y. Y. Xi, Y. F. Hsu, A. B. Djurisic and W. K. Chan, *J. Electrochem. Soc.*, 2008, **155**, D595.
179 Z. G. Chen, Y. W. Tang, L. S. Zhang and L. J. Luo, *Electrochim. Acta*, 2006, **51**, 5870.
180 T. Oekermann, T. Yoshida, H. Tada and H. Minoura, *Thin Solid Films*, 2006, **511–512**, 354.
181 H. Minoura and T. Yoshida, *Electrochemistry*, 2008, **76**, 109, permission to publish granted.
182 T. Yoshida, J. B. Zhang, D. Komatsu, S. Sawatani, H. Minoura, T. Pauporte, D. Lincot, T. Oekermann, D. Schlettwein, H. Tada, D. Wohrle, K. Funabiki, M. Matsui, H. Miura and H. Yanagi, *Adv. Funct. Mater.*, 2009, **19**, 17, permission to publish granted.
183 T. Oekermann, T. Yoshida, H. Minoura, K. G. U. Wijayantha and L. M. Peter, *J. Phys. Chem. B*, 2004, **108**, 8364.
184 X. Y. Gan, X. M. Li, X. D. Gao, X. L. He and F. W. Zhuge, *Mater. Chem. Phys.*, 2009, **114**, 920.
185 F. Labat, I. Ciofini, H. P. Hratchian, M. Frisch, K. Raghavachari and C. Adamo, *J. Am. Chem. Soc.*, 2009, **131**, 14290.
186 H. Graaf, C. Maedler, M. Kehr and T. Oekermann, *J. Phys. Chem. C*, 2009, **113**, 6910.
187 O. Lupan, V. M. Guerin, I. M. Tiginyanu, V. V. Ursaki, L. Chow, H. Heinrich and T. Pauporte, *J. Photochem. Photobiol., A*, 2010, **211**, 65, permission to publish granted.
188 F. Xu, Y. N. Lu, Y. Xie and Y. F. Liu, *J. Solid State Electrochem.*, 2010, **14**, 63.
189 F. Xu, Y. N. Lu, L. T. Sun and L. J. Zhi, *Chem. Commun.*, 2010, **46**, 3191.
190 F. Xu, L. T. Sun, M. Dai and Y. N. Lu, *J. Phys. Chem. C*, 2010, **114**, 15377, permission to publish granted.
191 L. F. Xu, Y. Guo, Q. Liao, J. P. Zhang and D. S. Xu, *J. Phys. Chem. B*, 2005, **109**, 13519.
192 L. F. Xu, Q. W. Chen and D. S. Xu, *J. Phys. Chem. C*, 2007, **111**, 11560, permission to publish granted.
193 F. Xu, Y. N. Lu, Y. Xie and Y. F. Liu, *Mater. Des.*, 2009, **30**, 1704.
194 M. Y. Zhong, H. Wang, Y. Liu, M. Li, H. Huang and H. Shen, *Chin. Sci. Bull.*, 2010, **55**, 1945, permission to publish granted.
195 S. B. Ambade, R. S. Mane, A. V. Ghule, M. G. Takwale, A. Abhyankar, B. W. Cho and S. H. han, *Scr. Mater.*, 2009, **61**, 12.
196 C. F. Lin, H. Lin, J. B. Li and X. Li, *J. Alloys Compd.*, 2008, **462**, 175, permission to publish granted.
197 C. H. Ku and J. J. Wu, *Nanotechnology*, 2007, **18**, 505706, permission to publish granted.
198 S. Yodyingyong, Q. F. Zhang, K. Park, C. S. Dandeneau, X. Y. Zhou, D. Triampo and G. Z. Cao, *Appl. Phys. Lett.*, 2010, **96**, 073115.
199 D. I. Suh, S. Y. Lee, T. H. Kim, J. M. Chun, E. K. Suh, O. B. Yang and S. K. Lee, *Chem. Phys. Lett.*, 2007, **442**, 348.
200 H. M. Cheng, W. H. Chiu, C. H. Lee, S. Y. Tsai and W. F. Hsieh, *J. Phys. Chem. C*, 2008, **112**, 16359, permission to publish granted.
201 F. Xu, M. Dai, Y. N. Lu and L. T. Sun, *J. Phys. Chem. C*, 2010, **114**, 2776, permission to publish granted.
202 F. Xu, Y. N. Lu, L. L. Xia, Y. Xie, M. Dai and Y. F. Liu, *Mater. Res. Bull.*, 2009, **44**, 1700.
203 Y. Z. Zheng, X. Tao, L. X. Wang, H. Xu, Q. Hou, W. L. Zhou and J. F. Chen, *Chem. Mater.*, 2010, **22**, 928, permission to publish granted.